Palaeogeography, Palaeoclimatology, Palaeoecology
January 2024, Volume 633, Pages 111884 (15p.)
https://doi.org/10.1016/j.palaeo.2023.111884
https://archimer.ifremer.fr/doc/00859/97062/

Last Glacial – Holocene variability of the European Slope Current, NE Atlantic

Depuydt P. [1, *], Toucanne Samuel [2], Barras C. [1], Le Houedec S. [1], Mojtahid M. [1]

[1] University of Angers, Nantes and Le Mans, CNRS, UMR 6112, Laboratoire de Planétologie et Géosciences, F-49000 Angers, France
[2] University of Brest, CNRS, Ifremer, Geo-Ocean, F-29280 Plouzané, France

* Corresponding author : P. Depuydt, email address : pauline.depuydt@laposte.net

Abstract :

The upper branch of the Atlantic Meridional Overturning Circulation (AMOC) in the mid-latitudes of the Northeast Atlantic remains poorly studied. This study provides a complete overview of the glacial, deglacial and Holocene dynamics of the easternmost portion of the AMOC upper branch, namely the European Slope Current (ESC) and its glacial equivalent known as the Glacial Eastern Boundary Current (GEBC). This is achieved through the study of the sediment core SU81–44 retrieved from the southern Bay of Biscay (BoB) (~1000 m water depth), and by using a multiproxy approach (i.e. benthic foraminiferal assemblage, grain size proxies, oxygen and carbon stable isotopes, and neodymium isotopic composition of foraminiferal shells). During the glacial period and the onset of the deglaciation, the grain size proxies at SU81–44 fluctuate significantly. These fluctuations are coherent with changes in relative densities of benthic foraminiferal indicator species of current strength and ventilation, thus highlighting significant changes in the GEBC vigor through time. The SU81–44 data confirm the Dansgaard-Oeschger interstadial/faster-stadial/slower flow pattern previously observed in northern BoB. Our results also provide new constraints on the strength of the slope current during the late deglaciation and Holocene period with a significant reinvigoration of the ESC, and by extension the upper branch of the AMOC during the Bølling-Allerød warming. This seems to confirm the crucial role of the ESC in deep water formation at high northern latitudes, as it is the case today. Finally, our data show a progressive weakening of the ESC during the Holocene. We hypothesize a link with a long-term decrease in the density gradient between low and high latitudes that can be attributed to long term changes in insolation and the strength of the subpolar gyre dynamics.

Highlights

► We present a continuous record of the European Slope Current for the last 36 kyr. ► The slope current intensity peaks during the Bølling-Allerød then gradually decreases throughout the Holocene. ► Changes in the meridional density gradient likely explain slope current changes. ► Reappearance of the Mediterranean water in the southern Bay of Biscay at ~16 ka.

Keywords : Late Glacial, Heinrich Stadials, Bølling–Allerød, Holocene, European Slope Current, Northeast Atlantic, AMOC

1. Introduction

The Atlantic Meridional Overturning Circulation (AMOC) plays a central role in the distribution of heat to the high latitudes, and changes in its dynamics are responsible for climate oscillations through time (Broecker, 1991; Rahmstorf, 2002). During glacial periods, the AMOC strength was sensitive to episodic freshwater inflows from the melting of Northern Hemisphere ice sheets (Broecker and Denton, 1990; McManus et al., 2004; Lynch-Stieglitz, 2017) such as the Laurentide Ice Sheet (LIS) covering the North American continent, and the European Ice Sheet (EIS), covering northern Europe (Ehlers et al., 2011). For example, during the last glacial period (74-11.7 ka; all ages are reported in calendar age before present) and the onset of the last deglaciation (*i.e.* Termination I, from *ca* 19 ka; Clark et al., 2012), large amounts of icebergs and meltwater were released into the North Atlantic (*e.g.* Ruddiman and McIntyre, 1981; Bond et al., 1992; Zaragosi et al., 2001), resulting in significant and recurrent weakening of the AMOC (Vidal et al., 1997; Denton et al., 2010; Ivanovic et al., 2018; Ng et al., 2018). These periods of AMOC weakening were concomitant with very cold climate intervals (*i.e.* Heinrich Stadials - HS) detected in Greenland ice cores (Dansgaard et al., 1993), North Atlantic marine records (Bond et al., 1993), as well as in numerous European and North American continental records (*e.g.* Grimm et al., 1993; Sanchez Goñi et al., 2002).

Several studies have highlighted the importance of the upper branch of the AMOC (above ~1000 m water depth) on rapid glacial climate fluctuations (*e.g.* Lehman and Keigwin, 1992; Chapman and Shackleton, 1998; Rasmussen and Thomsen, 2004) since the northward transport of heat and salt plays a fundamental role in ocean-cryosphere oscillatory mechanisms (Webb et al., 1997; Shaffer et al., 2004; Arzel et al., 2010; Peltier and Vettoretti, 2014; Saha, 2015; Boers et al., 2018). Nevertheless, the study of the upper branch of the AMOC during the last glacial period and Termination I remains poorly documented and mainly restricted to the Nordic Seas and the Atlantic inflow (*e.g.* Rasmussen and Thomsen, 2004; Moffa-Sánchez et al., 2019). Recent studies from the northern Bay of Biscay (BoB; Northeast Atlantic; Figure 1) revealed that the upper branch of the AMOC has strongly affected the European Atlantic margin during the last glacial period, compared to the Holocene, through the reinforcement of the northward-

flowing Glacial Eastern Boundary Current (GEBC; Toucanne et al., 2021; Depuydt et al., 2022), that is a glacial version of the modern European Slope Current (Pingree and Le Cann, 1989, 1990; Moritz et al., 2021). These findings highlight strong basin-scale changes in the glacial North Atlantic (*i.e.* changes in meridional density gradients), in agreement with previous numerical approaches that suggest that the North Atlantic Current (NAC) flowed zonally and further south than at present (as far south as ~40°N) during the last glacial period (*e.g.* Keffer et al., 1988; Otto-Bliesner et al., 2006; Brady and Otto-Bliesner, 2011). This makes the European Atlantic margin, and the upper slope environments in particular, a suitable region for glacial AMOC reconstructions. Here, we provide a new sedimentary and biotic record from the southern BoB that target a more southern location than previous studies (*e.g.* Peck et al., 2006, 2007; Toucanne et al., 2021; Depuydt et al., 2022) along the European margin (Southern BoB) to better constrain the spatial variability of the slope current dynamics. Our study further provides, for the first time in the region, a continuous slope current record, covering the final part of the last glacial period, the Termination 1 and the Holocene (*i.e.* last 11.7 ka). The use of sedimentological (grain size and X-ray fluorescence) data, benthic foraminiferal assemblages, and foraminiferal-based geochemical proxies (oxygen, carbon and radiogenic neodymium isotopes) reveal significant, regional-scale fluctuations in the strength and source of the slope current during the last 36 kyrs, in concert with the millennial climate variability of the last glacial period. Our data also suggest an overshoot in the strength of the slope current during the Bølling–Allerød interstadial, then an overall decrease of the ESC vigor throughout the Holocene, possibly linked to long-term changes in insolation and the Subpolar Gyre dynamics.

2. Geological and hydrographic setting

2.1. Geological setting

The BoB is an oceanic embayment located in the Northeast Atlantic, bordered to the east and south by the French (*i.e.* Celtic, Armorican, and Aquitanian) and Spanish (*i.e.* Galician, Asturian and Cantabrian) margins, respectively (Figure 1a). The Celtic-Armorican margin is up to 300-1000 km wide with a continental slope dominated by submarine canyons (Bourillet et al., 2001, 2006). The Aquitanian margin is much narrower (30-80 km) and the slope is smooth and extended by the marginal Landes Plateau (where the sediment core studied here was retrieved; Figure 1), dipping gently westward (Bourillet et al., 2006; Mulder et al., 2012). Two main canyons border the Landes Plateau, namely the Cap-Ferret Canyon and the Capbreton Canyon mainly fed by the Gironde and Adour rivers, respectively (Figure 1b).

2.2. Modern and past hydrological setting

The modern BoB is under the influence of the surface circulation and the anticyclonic eddies shed from the slope current, named Slope Water Oceanic eDDIES (SWODDIES; Pingree and Le Cann, 1992) (Figure 1a). The SWODDIES can extend until ~600 m depth (Le Groupe Tourbillon, 1983) and stimulate the mixing of water mass and exchange of their properties (*e.g.* temperature and salinity) and nutrient contents, from the shelf and slope regions (Ferrer and Caballero, 2011). The origin of the BoB surface water is the Eastern North Atlantic Central Water (formed in the intergyre zone; Pollard et al., 1996), that can be recognized down to ~600 m depth (van Aken, 2000).

At intermediate depth (~600-1300 m), the Mediterranean Outflow Water (MOW) is the dominant water mass (van Aken, 2000). The MOW is formed at Gibraltar Strait by the overflow of saline water from the Mediterranean Sea (van Aken, 2000) and is transported into the BoB (until ~50°N; Iorga and Lozier, 1999) by the European Slope Current (ESC; Huthnance, 1986; Pingree and Le Cann, 1989). The ESC represents the easternmost portion of the upper branch of the AMOC (Huthnance et al., 2020) and is forced by the topography of the European margin, the meridional density gradients and the wind forcing drive geostrophic flows towards the slope and then divert poleward (Huthnance, 1984; Friocourt et al., 2007; Marsh et al., 2017). Marsh et al. (2017) recently demonstrated that fluctuations of the ESC strength reflect the variability of the strength of the Subpolar Gyre (SPG). The pathway of the ESC ends in the Feroe-Shetland Channel (~60°N), where it forms, together with the North Atlantic Current (NAC), the Norwegian Atlantic Slope Current (Orvik and Niiler, 2002), that is a major part of the AMOC upper branch (down to 1500 m depth ; Lozier et al., 2019; Huthnance et al., 2020). A significant part of the latter reaches convection sites and participates to the formation of the North Atlantic Deep Water (NADW) which flows southward between 2000 and 4000 m (Dickson and Brown, 1994).

3. Material and methods

Core SU81-44 (4.37 m long, 1173 m water depth) was collected from the Landes Plateau (44°15.4'N 2°41.7'W) during the CEPAG campaign onboard the *R/V* Le Suroît (Duplessy, 1981). The core is composed of homogeneous silty-clay sediments. The study focuses on the

upper (undisturbed) ~350 cm of the core (Figure S1) as coring disturbances are evident in the lower part of the record (as highlighted by X-ray images; Figure S2).

3.1. Chronostratigraphy

The chronological framework for core SU81-44 is based on the synchronization (via 19 tie-points; Table S1) of the Ca/Ti ratio (obtained through X-ray fluorescence -XRF) with the well-dated core MD95-2002 (Figure 2b) using the approach detailed in Toucanne et al. (2021). This approach was successfully used to establish the age model of core BOBGEO-CS05 (Depuydt et al., 2022), which is compared to core SU81-44 later in this study. The age model of core SU81-44 is validated by 12 radiocarbon (^{14}C) dates (measured on monospecific or bulk planktonic foraminifera and performed at LMC14, France; Figure S1 and Table S2) and the recognition of ice-rafted detritus (IRD)-rich layers (visible on X-ray images; Figure 2d) deposited during the so-called Heinrich events (HE), *i.e.* short-lived events of massive iceberg discharges in the subpolar North Atlantic (Heinrich, 1988; Hemming, 2004). Nevertheless, the overall low occurrence of IRD observed in core SU81-44 compared to the northern records indicates that icebergs did not or rarely reach our study site. This may be due to the long distance of the study area from the icebergs melting area or to surface currents that prevent icebergs from massively reaching our area. Still, because there are some few IRD during Heinrich Event 1 (HE1; Figure 2d), we suppose that icebergs have reached our site at the time, due to a more extended ice cover. Finally, the abundance (%) of the polar planktonic taxon *Neogloboquadrina pachyderma* in core SU81-44 was compared to those of cores MD95-2002 (Grousset et al., 2000) and BOBGEO-CS05 (Depuydt et al., 2022) (Figure 2c). The striking resemblance between the three datasets (despite the low resolution for core SU81-44) confirms the reliability of the XRF-based synchronization. This approach reveals that core SU81-44 covers the last ~36 kyr, thus encompassing the final part of the last glacial period (including the last three HSs,during which the HE occurred), the Termination 1 and the Holocene period.

3.2. Foraminiferal data

For benthic foraminiferal assemblage analysis, core SU81-44 was sampled every 5 to 20 cm (1cm-large sections, n = 65, with an average resolution of ~1300 years during the Holocene and ~400 years during the glacial period). All samples were first weighted wet then dried after putting them in a 50°C oven. Then, all samples were washed over 63 µm and 150 µm sieves. The >150 µm fraction was split with a dry Otto microsplitter when necessary, until at least 250-

300 specimens were obtained in the final split. The samples with low densities were picked entirely (Table S3). Then, specimens from the >150 µm fraction were picked and mounted on Plummer cell slides for taxonomic determination. Following the protocol proposed by Depuydt et al. (2023), we assessed the composition of the small fraction (63 - 150 µm) through the study of 15 out of the 65 samples (selected strategically based on major sedimentological and foraminiferal (>150 µm) changes). These samples were split with a dry Otto microsplitter until a minimum of 150 individuals were obtained in the final split. Four out of the 15 samples were picked, put on Plummer cell slides and determined. For the rest of the samples, foraminifera were counted and determined directly major species under the stereomicroscope. The relative abundances of benthic foraminifera (% of total abundance) were calculated for all samples and the error bars were computed with the binomial standard error $\frac{\sqrt{(p\,(1-p))}}{n}$ (Buzas, 1990; Fatela and Taborda, 2002), where *p* is the species proportion estimate (number of counted individuals for a given species/*n*) and *n* is the total number of specimens. The benthic foraminiferal accumulation rates (BFAR; ind.cm^{-2}.ka^{-1}) were calculated as : number of individuals per gram of dry sediment x linear sedimentation rate (cm.ka^{-1}) x dry bulk density (g.cm^{-3}) (Herguera and Berger, 1991). The Dry Bulk Density (DBD) was calculated after Auffret et al. (2000) and following the relation: DBD = 2.65 x (1.024 – wet density)/(1.024-2.65), where 2.65 g.cm^{-3} is the grain density, and 1,024 g.cm^{-3} is the interstitial water density. The wet density was estimated from the wet weight and the volume of each subsample. Because our sediment core was sampled over 40 yrs ago, absolute BFAR values should be taken with caution and interpretations should be mainly based on relative variations. Nonetheless, the preservation seems to be optimal since the obtained average wet density value of 1.8 g.cm^{-3} is coherent the average density of marine sediments of 1.7 g.cm^{-3} published by Tenzer and Gladkikh (2014).

The diversity of the 65 samples of the >150 µm fraction was calculated using PAST software (Paleontological Statistics; Version 2.14; Hammer et al., 2001) to determine the Shannon index (entropy, H'; Hayek and Buzas, 1997) according to the equation $H' = -\sum i\ pi.\ln(pi)$ where p is the proportion of the ith species (p = %/100). Error bars representing 95 % of the confidence interval were computed with a bootstrap procedure.

In this study, we discuss particularly species >10 % in both size fractions that exhibit significant variability. Some of these species, and especially their general evolution between glacial and deglacial/Holocene periods, were included in the comparative study of Depuydt et al. (2023) on the effect of the chosen size fraction. Paleo-interpretations of benthic habitats are

based mostly on studies addressing modern benthic foraminiferal ecology in the BoB (*e.g.* Caralp et al., 1970; Pujos, 1972; Fontanier et al., 2002, 2003, 2006; Duchemin et al., 2008; Pascual et al., 2008; Mojtahid et al., 2010; Martínez-García et al., 2013).

Principal component analyses (PCA) was performed on the species with abundances >10 % of the total assemblage, using the variance-covariance matrix in PAST software (Paleontological Statistics; Version 2.14; Hammer et al., 2001).

The planktonic taxon *N. pachyderma* was counted for 22 samples from the >150 µm fraction, where relative abundances were determined in a single sample split with at least 300 planktonic individuals.

3.3. Sedimentology: X-ray images and grain-size measurements

2D X-ray images were acquired with a Geotek XCT system (Ifremer, Brest) from split core sections (Figure S2). Grain-size analyses ($n = 113$) were performed with a Mastersizer 3000 laser diffraction particle size analyzer coupled to a Hydro LV wet dispersant unit (Ifremer, Brest). Sediment samples were acidified beforehand with 1N acetic acid to remove the biogenic carbonate fraction, then rinsed with Milli-Q water. Near-bottom current flow speed are commonly reconstructed using the Sortable Silt ($\overline{SS}$; $10 - 63\ \mu m$) proxy of McCave et al., (1995). In core SU81-44, the $\overline{SS}$ fraction (or %SS) is low (*i.e.* ~34 ±3 % with 40 % maximum), excluding the use of $\overline{SS}$ to reconstruct the strength of the slope current. Instead, we used both the UP10 proxy (*i.e.* percentage of grains >10 µm) of Frigola et al. (2007, 2008) and the silt/clay ratio (Hall and McCave, 2000). These constitute relevant alternatives for paleoflow reconstructions (see Frigola et al., 2007 for a thorough discussion). We also calculated the median particle size D_{50} (*i.e.* 50th percentile).

3.4. Inorganic Geochemistry

3.4.1. X-ray fluorescence data

The relative abundances of the major elements calcium (Ca) and titanium (Ti) were obtained using an Avaatech X-ray fluorescence (XRF) scanner (Ifremer, Brest). XRF data were collected every 1 cm along the entire length of the core with a counting time of 10 s, setting the voltage to 10 kV (no filter) and 30 kV (Pd thick filter) and the intensity to 600 and 1000 µA,

respectively. Results are presented in logarithmic ratios of element intensities (Weltje and Tjallingii, 2008).

3.4.2. Oxygen, carbon and neodymium isotopes

For carbon and oxygen stable isotope analyses ($\delta^{13}C$ and $\delta^{18}O$ as ‰ VPDB), 52 benthic foraminiferal samples were measured every 3 to 26 cm (depending on the sedimentation rate, with an average resolution of ~1760 years during the Holocene and ~530 years during the glacial period). These analyses were obtained on 2 to 8 specimens of *Cibicidoides kullenbergi*/*pachyderma*, hand-picked from the >150 µm fraction. $\delta^{13}C$ and $\delta^{18}O$ were measured at the Pôle Spectrométrie Océan (IUEM, Brest) using a MAT 253 (Thermo Scientific) isotope ratio mass spectrometer coupled with a KIEL IV Device (Thermo Scientific) to transform carbonates in gas. The standard deviation analytical precision is calculated using an in-house homogeneous calcite standard. It is ± 0.03 ‰ for $\delta^{18}O$ and ± 0.02 ‰ for $\delta^{13}C$ for this range of mass (120-250 µg). To formulate the values in the V-PDB scale, all samples were calibrated using two international carbonate standards: NBS-19 ($\delta^{18}O$ = -2.20 ‰ and $\delta^{13}C$ = 1.95 ‰) and NBS-18 ($\delta^{18}O$ = -23.20 ‰ and $\delta^{13}C$ = 5.01 ‰).

To investigate the evolution of the isotopic signature of bottom water masses, radiogenic isotopes of neodymium (ε_{Nd}) were measured on 31 samples of planktonic foraminiferal shells (from 8 to 30 mg). Detrital materials were removed with sonication in double distilled water several times, then crushed shells were dissolved using acetic acid following the procedure described in (Tachikawa et al. (2014). The neodymium content of foraminiferal shells was extracted following the two steps columns procedure described in Bayon et al. (2012). The isotopic measurements were performed at the Pôle Spectrométrie Océan (IUEM, Brest) using a Thermo Scientific Neptune ICPMS multi-collector. Nd isotopic compositions were determined using a sample-standard frame with internal standard solution (SPEX-Nd) analyzed every two samples. Nd isotope ratios were corrected for mass discrimination by normalising to $^{146}Nd/^{144}Nd = 0.7219$ using an exponential law. In addition, the isotopic ratios were normalised to $^{143}Nd/^{144}Nd = 0.512115$ for the JNdi-1 certified Nd standard (Tanaka et al., 2000). Analyses were monitored using JNdi-1 standard solutions at concentrations similar to those of the measured samples (25 ppb) giving $^{143}Nd/^{144}Nd$ of 0.512071 ± 0.000038 (2σ, n = 7) corresponding to an external reproducibility of ~±0.74 ε_{Nd} (2σ). The Nd isotopic ratios are

expressed with the epsilon notation (ε_{Nd}) calculated using the $^{143}Nd/ ^{144}Nd$ chondritic reservoir value (CHUR) of 0.512630 (Bouvier et al., 2008).

4. Results

4.1. Benthic foraminifera

4.1.1. >150 µm size fraction

The BFAR values vary around ~700 ind.cm^{-2}.ka^{-1} (Figure 3a) Minimum BFAR values are found during each HS (~500 ind.cm^{-2}.ka^{-1}), between HS2 and HS3 and at ~21 ka. The highest BFAR values (>1000 ind.cm^{-2}.ka^{-1}) are found before HS3, at the onset of the LGM, during late HS1, and during the Holocene.

The Shannon index varies between 1.5 to 2.5 with an average of 2 along the record (Figure 3b). Minimal values are recorded during the early part of HS2 (at ~25.3 ka), at the onset of the LGM (at ~22.6 ka), and during early HS1 (at ~17.4 ka). The highest values are observed during HS3, late HS2 (at ~23.9 ka), late HS1 (at ~16 ka), and most of the LGM and the Holocene.

Based on the PCA analysis (Figure S3), species >10 % of the total assemblage can be separated into two main groups:

i) The glacial assemblage is dominated by two main species: *Cibicidoides pachyderma* with relative abundances varying between 10 and 70 % (Figure 3c), and *Sigmoilopsis schlumbergeri* varying between ~0 and 30 % (Figure 3d). Both species show a comparable evolution through time with an overall increase in percentages from 36 ka to early HS2 and the onset of the LGM where they reach their maximum percentages. After, an overall decrease is recorded until reaching minimum values during the Holocene. *Cibicides wuellerstorfi* (0 - 17 %; Figure 3j), *Quinqueloculina* spp. (1 - 10 %; Figure 3k), *Gavelinopsis praegeri* (0 - 8 %) (Figure 3**Figure**m) and *Gyroidina orbicularis* (0 - 10 %; Figure 3n) record their lowest abundances during HS1 and HS2. During HS3, some of these species (*i.e. C. wuellerstorfi* and *G. orbicularis*) are present with high abundances. *Globobulimina* spp. (1 - 35 %; Figure 3g), *Bolivina albatrossi* (0 - 12 %; Figure 3h) and *Bulimina* spp. (0 - 20 %; Figure 3i) show abrupt increases during HS2 and early HS1, with values up to 40 %, 10 % and 15 % respectively.

ii) The deglacial/Holocene assemblage is mainly dominated by *Uvigerina mediterranea* (Figure 3e) and *Uvigerina peregrina* (Figure 3f) with relative abundances varying between 10 and 55 % and 10 and 20 % respectively. Both appear during the last deglaciation and are highly abundant

during the Holocene. *Melonis affinis* (5 - 11 %; Figure 3l) is abundant during the Holocene and nearly absent during the last glacial period except at the start of the record and at HE3.

4.1.2. >63 µm size fraction

When considering the small size fraction, the composition of the total assemblage (>63 µm = 63-150 µm + >150 µm) is different from the >150 µm fraction and it is largely dominated by *Cassidulina carinata* during the last glacial period with relative abundances of ~65 % on average (Figure 3o), whereas the abundance of *C. pachyderma* becomes minor (Figure 3c). Additionally, new (and/or rare in the >150 µm fraction) taxa are found to be dominant in the >63 µm fraction: *Trifarina angulosa*, nearly absent in the large fraction, is dominant (10-15 %) during HS2 and late HS1 (Figure 3q). *Alabaminella weddellensis* and *Epistominella exigua* are exclusively present in the small size fraction (Figure 3p) and show the same trend as the uvigerinids with values around 25 % and 5 % from the end of HS1, respectively.

4.2. Sedimentological and geochemical results

4.2.1. Sedimentological proxies

Grain size measurements of the carbonate-free fraction shows that most samples are unimodal, with a mode value at ~7 µm (Figure 4b). There are few samples showing a bimodal distribution with a second mode around 100 - 230 µm, when the median grain size (D_{50}) increases abruptly, *i.e.* at 27.2 and 24.2 ka (Figure 4c). Most of D_{50} values vary between 6 and 7 µm, but peaks at 8.5 to 10 µm occur at 30.7, 27.2 and 24.2 ka. The lowest D_{50} values (*i.e.* <6 µm) occur during early HS1 (*i.e.* 18 – 16.7 ka), HS2 (*i.e.* 26 – 23 ka) and the end of HS3 (*i.e.* 30 – 29 ka). These minimum values are followed by rapid increases in the D_{50} value, reaching a maximum at 12.8 ka, followed by a gradual decrease during the Holocene. The average values of UP10 and silt/clay ratios are 37 ± 2.6 % and 7.6 ± 0.1, respectively, and follow the same trend as the D_{50} record (Figure 4c).

4.2.2. Bottom-water chemical signature

The benthic $\delta^{13}C$ data values vary around an average value of ~0.9 ± 0.1 ‰. Minimal values of 0.8 ‰ and 0.4 ‰ are found at the end of HS2 and HS1 respectively (Figure 4f). Benthic $\delta^{18}O$

values fluctuate between ~2.5 to ~3 ‰ during the glacial period before an abrupt decrease from 18.2 ka (*i.e.* early HS1) reaching values of 2 ‰ (Figure 4e), values which are maintained during the Holocene.

Glacial ε_{Nd} values of benthic foraminifera are around -8.7 ± 0.5 (n = 14) until 20 ka (Figure 4d). After 20 ka, the ε_{Nd} values decreased rapidly to reach a minimal value of -11.7 ± 0.3 at 16.9 ka. After, ε_{Nd} values increased to reach ~-10.2 ± 0.7 (n = 5) at 14 ka and during the Holocene.

5. Discussion

5.1. Paleoceanographic significance of the SU81-44 dataset

The sedimentological paleocurrent sensitive proxies (UP10, silt/clay ratio) at site SU81-44 showed significant fluctuations during the last 36 kyr. These fluctuations are concomitant with the main climate changes recognized over this period, including the abrupt Dansgaard-Oeschger (D-O) oscillations, thus highlighting a strong climatic/oceanographic forcing on the sedimentary characteristics of the Landes Plateau. Typically, low grain size values characterize the HSs (HS3, HS2 and HS1) and the Late Holocene (*i.e.* last 4 kyr), while coarser sediments characterize D-O interstadials (namely Greenland Interstadials-GI) GI7 to GI5.2, GI3, the mid-HS2 event and the Bølling-Allerød (Figure 4). The relative abundances of *Trifarina angulosa*, an indicator species of high-bottom energy regimes (Mackensen et al., 1985; Austin and Evans, 2000; Gooday and Hughes, 2002), mimics the grain size variability through a positive relationship (*i.e.* higher abundance of *T. angulosa* correlates to coarser grain size) (Figure 5a). Furthermore, the evolution of both abiotic (*i.e.* UP10, silt/clay ratio, and D_{50}) and biotic (*i.e. T. angulosa*) data from core SU81-44 is coherent with the glacial slope paleoflow (*i.e.*, GEBC) reconstruction of Toucanne et al. (2021) from the northern BoB (~1,000 m depth; Figure5a). Therefore, we assume that the grain size variability at site SU81-44 is controlled by changes in near-bottom flow speed, and that site SU81-44 record the strength of the GEBC during the last glacial period in concert with the sites from the northern BoB (Toucanne et al., 2021; Depuydt et al., 2022).

Nowadays, mean velocities of the slope current, namely the ESC, increase poleward (Huthnance, 1986; Pingree and Le Cann, 1989, 1990). During the last glacial period, we assume that this was also the case, since we record a significant difference in the average grain size between the southern (fine-grained sediments; mean UP10 of 37.4 ± 3.2, *n*=101) and the northern BoB slope (coarse-grained sediments; *e.g.* at site BOBGEO-CS05, with a mean UP10

of 68.3 ± 6.9, *n*=148). Nevertheless, part of this difference can be also explained by the steeper slope in the northern BoB influencing the current velocity. It is interesting to note that these oceanographic and physiographical features along the BoB margin also affects the size of some benthic foraminiferal species, including the high-energy indicator *T. angulosa*. The latter dominates the >150 µm size fraction in the northern BoB (Mojtahid et al., 2017; Depuydt et al., 2022) while it mostly occupies a finer fraction (63-150 µm) at SU81-44 site (Depuydt et al., in press). This indicates that benthic foraminiferal species are capable of displaying different types of ecological strategies depending on the environmental conditions at the seafloor (*e.g.* quality and quantity of organic matter, velocity of currents; see Depuydt et al., 2023, for a thorough discussion).

We found similar ε_{Nd}, benthic $\delta^{13}C$ and benthic $\delta^{18}O$ values for both this site and the northern BoB (Toucanne et al., 2021) (Figure 5). This highlights a homogeneous intermediate water mass flowing all along the BoB upper slope, especially during the glacial period, most likely transported by the GEBC. Until now, the nature of the glacial intermediate water mass moving northward by the GEBC remained elusive. Nowadays, the ESC at the BoB latitude, mainly transports the MOW, which is found up to ~50°N (south Porcupine Bank; Iorga & Lozier, 1999; McCartney & Mauritzen, 2001). This modern configuration is reported for the whole Holocene, as suggested by coral- (Copard et al., 2011; Boavida et al., 2019) and foraminifera-based (Mojtahid et al., 2015; Depuydt et al., 2022) studies from the BoB. The ε_{Nd} values of planktonic foraminifera from core SU81-44 support this oceanographic pattern with a mean Holocene ε_{Nd} signature of -10.2 ± 0.7 (*n*=4; Figure 5), close to the values of -10.9 ± 0.3 and -11.2 ± 0.3 for both modern Mediterranean-sourced water off Portugal (at 1200 m water depth), and Holocene corals in the southern Bay of Biscay (at 1150-1200 m depth) (Piepgras and Wasserburg, 1983; Copard et al., 2011). Glacial (>20 ka) ε_{Nd} values are more radiogenic at both SU81-44 (-8.7 ± 0.5, *n*=14) and the northern BoB (-9.1 ± 0.4, *n*=35) sites (Figure 5), revealing a different regional paleohydrographic structure. During the LGM, the MOW was reduced in volume (Rogerson et al., 2012; Zahn et al., 1997) and flowed deeper (about 700 m deeper than today) due to higher salinity and colder temperatures of Mediterranean waters (Schönfeld and Zahn, 2000; van Dijk et al., 2018; Sierro et al., 2020). This MOW adjustment could explain the increased flow speed recorded on the lower slope at the LGM in the northern BoB (Toucanne et al., 2021). However, without any evidence for mor radiogenic MOW during glacial (*e.g.* Jimenez-Espeio et al., 2015), the glacial ε_{Nd} values observed at sites BOBGEO-CS05 and SU81-44 cannot be explained by the influence of the MOW at intermediate depth in

the BoB. On the other hand, such ε_{Nd} values most likely indicate a north Atlantic origin of the water mass similar to those found for the Nordic Seas overflow (ε_{Nd} ~ -8 to -10 ; Piepgras and Wasserburg, 1987; Lacan and Jeandel, 2004). In the northern BoB, the glacial ε_{Nd} values were attributed to recirculated northern-sourced waters transported eastward by the glacial NAC and ultimately entrained into the GEBC (Toucanne et al., 2021), as for the Labrador Sea Water today (Rhein et al., 2015; Zou and Lozier, 2016). Another possibility for the signature of the glacial water mass is the impact (through mixing) of low latitude water (*i.e.* subtropical gyre, where the NAC forms), where ε_{Nd} values range from -9 to -10 above ~1000 m water depth (van de Flierdt et al., 2016), but this assumption remains speculative and highlights, as a whole how complex the use of ε_{Nd} to trace MOW and other water masses in the BoB is (Stumpf et al., 2010). This is further confirmed, between ~20 and 17 ka, when enhanced continental inputs into the BoB most likely overwhelmed the oceanographic signal of isotopic signature (through reversible scavenging and/or sediment-seawater interactions; Jeandel and Oelkers, 2015; Blaser et al., 2019). Enhanced continental inputs are probably the result of the massive deglacial Channel River discharges (R4 event; Figure 5b) occurring at that time in the BoB. This is supported by coarser materials brought into the Landes Plateau area between 18 and 14 ka (Figure 4c) and by systematic unradiogenic values (down to -14;7) in the detrital ε_{Nd}record off the paleo Channel River mouth (Toucanne et al., 2015).

5.2 Glacial and Holocene dynamics of the slope current in the southern BoB: biotic and abiotic signals

5.2.1. Heinrich Stadials

At site SU81-44, the overall low values of bottom flow speed proxies (*i.e.* UP10, silt/clay ratio) indicate a weak GEBC during the three last HSs (Figure 4c). The decrease in the GEBC strength occurs well before the HEs, that usually occurred towards the end of the corresponding stadials (Figure 4c). Similar findings are reported from several sites along the French Atlantic margin and the northern BoB (Toucanne et al., 2021; Depuydt et al., 2022). A detailed look at the biotic data also reveals that HSs are characterized by low oxygen concentrations, as indicated by the systematic presence of *Globobulimina* spp. (less clear for HS3 due to the low sampling resolution), deep infaunal species tolerant to anoxia (*e.g.* Risgaard-Petersen et al., 2006; Pina-Ochoa et al., 2010; Koho et al., 2011). These observations

are in line with results obtained from the northern BoB sites (Mojtahid et al., 2017; Depuydt et al., 2022) suggesting an establishment of a pervasive sluggish bottom water circulation during HSs on the western European margin, and well before the triggering of the HEs. Because the GEBC is part of the upper branch of the AMOC, our new data also support the idea that AMOC weakening, likely triggered by the release of EIS meltwaters (*e.g.* Stanford et al., 2011; Toucanne et al., 2015; Ivanovic et al., 2018), precedes the destabilisation of the Hudson Strait Ice Stream and the subsequent HEs (Barker et al., 2015 and references therein). In addition, a sluggish circulation at that depth might also result from the deepening of the MOW during the Heinrich Stadials (van Dijk et al., 2018; Sierro et al., 2020). If correct, this scenario highlights a strong relationship in between the Atlantic-Mediterranean exchanges and the Northern Hemisphere climate changes (*e.g*. Cacho et al., 1999; Voelker et al., 2006).

Despite the above-mentioned common features, our SU81-44 foraminiferal record points out several specifics of each of the three HSs. A particular feature can be seen for HS2 during which our bottom flow speed proxies show a revigoration of the GEBC at 24.2 ka. This is also emphasised with a peak in the abundance of the high energy indicator species *T. angulosa*, while a concomitant increase in the abundance of the polar planktonic *N. pachyderma* indicates a warming of surface waters (Figure S6). These data reveal a rapid mid-HS2 reventilation event. This occurred at time of a well-known reorganization of the North Atlantic oceanic and atmospheric circulation (Rasmussen et al., 2008; Austin et al., 2012), of which the origin is still poorly understood. This rapid change has also been reported from the northern BoB records (Toucanne et al., 2021; Depuydt et al., 2022), confirming that both north and south BoB upper slope settings respond similarly to ocean-atmosphere-cryosphere dynamics, even at millennial timescales.

The detailed comparison of the three HSs of the SU81-44 record also reveals that HS1 and HS2 are characterised by the presence of both *Globobulimina* spp. and *Bulimina* spp., whereas *Globobulimina* spp., *M. affinis* and *C. wuellestorfi* dominate during HS3 (Figure S4). While *Globobulimina* spp. are low-oxygen indicator species, *Bulimina* spp. are usually found in highly eutrophic environments (Jorissen, 1987; Hermelin and Shimmield, 1990; Bernhard and Alve, 1996). *Melonis affinis* is an intermediate infaunal species considered as tolerating suboxia (Kaiho, 1994) and degraded organic matter (Fontanier et al., 2002) while *C. wuellerstorfi* is a suspension feeder living in well oxygenated environments (Mackensen et al., 1985; Bauch et al., 2001). Therefore, the combination of occurrences of *Globobulimina* spp. and *Bulimina* spp. suggests a higher export of organic fluxes to the seafloor during HS2 and HS1 than during HS3

in our study site, and that bottom waters during HS3 might have been better ventilated than during the other HSs as indicated by the higher abundance of *C. wuellerstorfi*. A better ventilation during HS3 is not coherent with sedimentological bottom flow speed proxies at our study site showing overall similar UP10 minima during HSs (Figure 5). This discrepancy between foraminiferal and sedimentological data might simply be the result of a lower organic flux during HS3 in the study site, limiting the consumption of oxygen. In the northern BoB site (BOBGEO-CS05; Figure 1) however, benthic foraminiferal assemblage distinguishes HS1 characterized by high organic fluxes from HS2 and HS3 where high organic indicator species were absent (Depuydt et al., 2022). Therefore, during HS3, low flux of organic matter characterized both northern and southern sites whereas the opposite was observed during HS1 (*i.e.* both settings experience high organic fluxes). During HS2, only the southern BoB records high organic matter fluxes to the sea floor. This is probably due to a different source of organic material leading to a local effect. Indeed, today the sedimentation of the study area is under the influence of the Adour-Garonne River system (*e.g.* Ruch et al., 1993; Jouanneau et al., 1999), and with them nutrients that trigger primary production (Borja et al., 2019). The Adour-Garonne River basin drains the Pyrenean chain and thus the dynamics of organic export in the ocean during HSs may have depended on the dynamics of the Pyrenean glaciers. The recent study of Allard et al. (2021) shows that Pyrenean glaciers retreated during HSs, in agreement with the warm Heinrich summers hypothesis of Denton et al. (2022). The study of Allard et al. (2021) further shows a difference in the glacial activity between HS1 and HS2 where a retreat was recorded, whereas during HS3, glaciers either stalled or retreated. This suggests that during HS3, the Garonne-Adour River system may have delivered less sediment (and therefore less nutrients and organic matter) to our study site than during HS2 and HS1. That said, and despite the dominant northward current direction, we cannot completely rule out that fine sediments originating from EIS meltwaters have reached our latitudes. Indeed, it could be especially true during early HS1 since it considered as a paroxysmal melting phase, when the estimated annual sediment load was ~25 times higher than that of the present-day rivers in the BoB (Toucanne et al., 2010). This might explain the concomitant peak of *Bolivina* spp. during early HS1, that is found in all foraminiferal records in the BoB (from north to south): MD99-2328 (Mojtahid et al., 2017), BOBGEO-CS05 (Depuydt et al., 2022), SU81-44 (this study) and PP10-12 (Pascual et al., 2020) (Figure S4 and Figure S5).

5.2.2. The deglacial period (19-11.7 ka)

During the deglacial period, the abundances of the uvigerinids (*U. peregrina* and *U. mediterranea*), that were nearly absent during the glacial period, increased significantly from ~15.5 ka (rapidly after HE1). This suggests that *Uvigerina* spp. have a stronger affinity to the interglacial configuration of surface productivity, *e.g.* nature of primary producers and seasonality in phytoplankton blooms (Schönfeld and Altenbach, 2005). This likely explains their near-absence during the glacial period, and their dominance during the Holocene and in the modern BoB between ~500 and 2000 m water depths (*e.g.* Schönfeld and Altenbach, 2005; Schönfeld, 2006; Barras et al., 2010; Mojtahid et al., 2010; Duros et al., 2011, 2012). The increase in their abundances starting from ~15.5 ka is coherent with the Iberian mid-slope records of Pascual et al. (2020) and Schönfeld and Altenbach (2005), showing a significant increase of uvigerinids from ~15.7 - 14 ka. In the northern BoB, Mojtahid et al. (2017) record the presence of the uvigerinids only in the Holocene portion of the record, but due to the poor preservation of the Holocene at their site (*i.e.* MD99-2328), the timing of their first appearance could not be constrained. In higher latitudes, Schönfeld and Altenbach (2005) observed the appearance of the uvigerinids at the Rockall Plateau later than at our study site, around 10 ka. Rüggeberg et al. (2007) observed a maximum abundance of *Uvigerina* spp. during the last 10 kyr at the Porcupine Seabight without specifying the timing of their appearance. Based on the above, there was probably a delay in their latitudinal settlements at intermediate depths in the Northeast Atlantic. Some studies hypothesized a link between the settlement of *Uvigerina* spp. in the BoB and the northward migration of the MOW with the deglacial sea-level rise and the concomitant increase in Mediterranean-Atlantic exchanges (Mojtahid et al., 2013; Depuydt et al., 2022). The maximum *Uvigerina* spp. abundance that we record at ~15.2 ka coincides with an increase in $\delta^{13}C$ data and a stable benthic foraminiferal $\delta^{18}O$ and ε_{Nd} values over the last 15 ka (Figure 5). This means potentially that a unique water mass was present between ~15.2 ka and late Holocene. The ε_{Nd} values support the hypothesis of a Mediterranean-sourced water in the BoB since 15 ka (see section 5.1). Therefore, we hypothesize a link between the high density of *Uvigerina* spp. and a strengthened flow of the MOW along the BoB slope. This would also explain the early appearance of the uvigerinids along the Iberian margin and the southern BoB compared to the higher latitudes, probably because of a progressive latitudinal settlement of uvigerinids associated to the gradual MOW expansion at intermediate depths of the Northeast Atlantic. In such a scenario, without excluding a change towards higher productivity during the warmer Holocene time period, the rise of the benthic $\delta^{13}C$ since 15 ka can also be interpreted as the northward's expansion of the warmer and more saline MOW

towards intermediate depths which, therefore, will improve the ventilation conditions at that site.

Bottom flow speed proxies from both the southern and northern BoB records (Figure 5a) show a rapid increase in the vigor of the slope current, and by extent that of the upper branch of the AMOC, in the second part of HS1 (*i.e.* after 17-16 ka). These observations in both southern and northern records of the BoB are evidence of regional signal, which is most likely linked to a oceanographic change. Our study further shows that this increase in the slope current attained a peak between 13.6 ka, coinciding with the mid- Bølling-Allerød (BA) interval and 12.0 ka that correspond to the mid-Younger-Dryas (YD) interval. This reinvigoration of the upper branch of the AMOC precedes by about 1.5 to 2 kyr the abrupt resumption of the deeper branch of the AMOC (>2400 m) in the western North Atlantic at the start of the BA warming ca. 14.7 ka (McManus et al., 2004; Ng et al., 2018). This AMOC "overshoot" during the BA warming occurs despite persistent deglacial meltwater fluxes that counteract vigorous North Atlantic deep-water formation(Liu et al., 2009). Modelling studies show that deglacial CO_2 rise and ice sheet decline modulate the sensitivity of the AMOC to these fluxes, as an alternative to or in combination with changes in the magnitude or routing of meltwater discharges (*e.g.* Barker et al., 2010; Sun et al., 2022). The reinforcement of the slope current in the Northeast Atlantic is coeval with increasing bottom water oxygenation and temperatures on the Celtic margin (Mojtahid et al., 2017), suggesting a subsurface warming that was transported northwards via the more vigorous slope current. This subsurface warming in the upper branch of the AMOC would have led to accelerated high latitude ice-sheet melting (Brendryen et al., 2022).

5.2.3. The Holocene (11.7-0 ka)

During the Holocene, benthic foraminiferal assemblages at SU81-44 show an overall increase in the abundances of the uvigerinids (*i.e. U. peregrina* and *U. mediterranea*), in agreement with the results obtained at the nearby site PP10-12 (Pascual et al.,2020) (Figure S6). The overall increase of these species abundances during the Holocene indicates a progressive enrichment in organic matter compared to the last glacial period (*e.g.* Fontanier et al., 2002; Mojtahid et al., 2010; Singh et al., 2015), which is consistent with the decrease in grain size at the studied site (Figure 5). Indeed, clay minerals favor the adsorption of organic matter (*e.g.* Keil et al., 1994; Bock and Mayer, 2000). Meanwhile, our bottom flow speed proxies show a decreasing trend through the Holocene (Figure 4c), indicating the strength of the ESC is most likely

progressively diminished. This long-term decrease in the ESC flow speed might be linked to a long-term change in oceanographic/climatic conditions. In the modern settings, the mechanisms controlling the ESC strength are mostly linked to meridional density gradients (Pingree and Le Cann, 1990; Friocourt et al., 2007; Marsh et al., 2017). Thus, the long-term decreasing flow speed of the ESC might be a result of a long-term weakening of this gradient. The early Holocene (before ~8 ka) was characterized by large cold freshwater inputs advected by the continuing melting of ice sheets in the high latitudes (*e.g.* Hillaire-Marcel et al., 2001; Thornalley et al., 2009). Conversely, due to increasing insolation, subtropical waters were likely warming. Therefore, we suggest that this increasing difference between low and high latitude settings established a high-density gradient, explaining the intense ESC recorded at SU81-44 during the early Holocene. Following the same logic, the decreasing insolation from mid-to late Holocene and the cessation of large freshwater inputs from the ice-sheets, would decrease this gradient and, by extension, the overall ESC strength. The hypothesis of a strong MOW influence seems to be contradictory with this decreasing ESC flow speed since the MOW production should increase due to a declining summer insolation (*e.g.* Bahr et al., 2015). Marsh et al. (2017) further showed a modern positive correlation between the intensity of the ESC and the dynamics of the SPG, *i.e.* strong (weak) transport is associated with to a strong (weak) SPG, with colder (warmer) water to the north setting up a stronger (weaker) northward density gradient. For the early Holocene, this link might not have been present due to a weakened SPG caused by advection of melting waters. As a result of this weakened SPG, Thornalley et al. (2013) hypothesized a weakened AMOC. Since the ESC is the easternmost branch of the AMOC, the vigorous slope current that we record would be inconsistent with this suggestion. That said, other studies report an active AMOC during the early Holocene (*e.g.* Hoogakker et al., 2011; McCave and Andrews, 2019; Sicre et al., 2021), in agreement with our observations along the European margin. Model simulations also show that the vigor of the AMOC is not simply related to sea-ice concentrations in the north Atlantic during periods of increasing atmospheric CO_2 (Zhang et al., 2017), such as the deglaciation and early Holocene. Increasing CO_2 affects the transport of atmospheric moisture across Central America, which modulates the freshwater budget of the North Atlantic and hence deep-water formation (Leduc et al., 2007; Zhang et al., 2017). From ~8 ka onwards, studies show an overall long-term contraction of the SPG and the AMOC (*e.g.* Colin et al., 2019; Thornalley et al., 2009, 2013), which, for this time period, would be coherent with the decreasing ESC vigor that we record. Thornalley et al. (2013) presented a stacked sortable silt record from the Reykjanes Ridge, which is indicative of the Iceland Scotland overflow strength (an important component of the deep branch of the

AMOC), and results reveal a decrease in its strength from mid to late Holocene, as for the ESC on the western European margin. This overall decrease paralleled the long-term westward contraction of the SPG from ~8 to 3 ka, superimposed on millennial-scale variability not observed in our data (likely due to the low temporal resolution) (Colin et al., 2019). Based on the above, we conclude that the link between SPG and ESC, and by extension AMOC, seems to be more straightforward after ~8 cal ka BP, probably because the advection of freshwaters form ice-sheets is no longer a primary forcing factor.

6. Conclusions

This study provides new constraints on the dynamics of the ESC, and on the associated benthic paleoenvironments characterizing the southern BoB over the last 36 ka. Our data show that:

- Upper slope paleocurrent dynamics reconstructed by sedimentological and foraminiferal proxies at site SU81-44, southern BoB, are in concordance with the northern BoB records, that all show paleoceanographic fluctuations in concert with the Northern Hemisphere climatic events. This shows a regionally consistent signal for the BoB that is strongly linked to a global climatic/oceanic forcing.
- During the last three HSs, our results show a slowing down of the GEBC and the consequent decreasing ventilation of bottom waters highlighted by the presence of low oxygen tolerant benthic foraminiferal taxa.
- The foraminiferal assemblages show some specificities to each HS. During HS2, when GEBC was weak in the BoB, our data indicate a short episode of GEBC reinvigoration around 24.2 ka similarly to the northern BoB.
- The appearance of uvigerinids in our record at around 15.5 ka may be an indication of the earliest post-glacial incursion of the MOW in the BoB.
- Our results show a peak in ESC vigor during the Bølling-Allerød, that we relate with the AMOC overshoot described at intermediate depths in the North Atlantic.
- Finally, our results showed a progressive decrease in the strength of the ESC during the Holocene, which could be partially related to a long-term decrease in the density gradient between high and low latitudes.

7. Acknowlegments

This study was financed by the CNRS-INSU-LEFE (IMAGO-CYBER) programme (STING project), the ARTEMIS ^{14}C AMS French INSU project, and the Region Pays de Loire programmes (Rising Star project TANDEM). S.T. was funded by the French National Research Agency (ANR) via the LabexMER program (ANR-10-LABX-19-01) and the PIA TANDEM project (ANR-11-RSNR-00023-01). Salary and research support for the PhD student (first author) were provided by the French Ministry of Higher Education and Research. We are very grateful to Elisabeth Michel (LSCE) for providing us with the studied sediment core and for her assistance with the writing. We are also thankful to F. Rihani, L. Dahhan (internship students) and S. Sanchez (University of Angers) for their help with benthic foraminifera picking, Fabien Dewilde (IUEM) for the $\delta^{18}O$ and $\delta^{13}C$ analyses and Germain Bayon (IFREMER) for his assistance with MC-ICPMS analyses. The raw data is available in the SEANOE data repository (https://doi.org/10.17882/91758).

8. References

Allard, J.L., Hughes, P.D., Woodward, J.C., 2021. Heinrich Stadial aridity forced Mediterranean-wide glacier retreat in the last cold stage. Nat. Geosci. 14, 197–205. https://doi.org/10.1038/s41561-021-00703-6

Arzel, O., Verdière, A.C. de, England, M.H., 2010. The Role of Oceanic Heat Transport and Wind Stress Forcing in Abrupt Millennial-Scale Climate Transitions. Journal of Climate 23, 2233–2256. https://doi.org/10.1175/2009JCLI3227.1

Auffret, G., Zaragosi, S., Voisset, M., Droz, L., Loubrieu, B., Pelleau, P., Savoye, B., Bourillet, J.-F., Baltzer, A., Bourquin, S., Dennielou, B., Coutelle, A., Weber, N., Floch, G., 2000. Premières observations sur la morphologie et les processus sédimentaires récents de l'Éventail celtique. Oceanologica Acta 23, 109–116. https://doi.org/10.1016/S0399-1784(00)00116-X

Austin, W.E.N., Evans, J.R., 2000. NE Atlantic benthic foraminifera: modern distribution patterns and palaeoecological significance. Journal of the Geological Society 157, 679–691. https://doi.org/10.1144/jgs.157.3.679

Austin, W.E.N., Hibbert, F.D., Rasmussen, S.O., Peters, C., Abbott, P.M., Bryant, C.L., 2012. The synchronization of palaeoclimatic events in the North Atlantic region during Greenland Stadial 3 (ca 27.5 to 23.3 kyr b2k). Quat. Sci. Rev. 36, 154–163. https://doi.org/10.1016/j.quascirev.2010.12.014

Bard, E., Rostek, F., Turon, J.-L., Gendreau, S., 2000. Hydrological Impact of Heinrich Events in the Subtropical Northeast Atlantic. Science 289, 1321–1324. https://doi.org/10.1126/science.289.5483.1321

Barker, S., Knorr, G., Vautravers, M.J., Diz, P., Skinner, L.C., 2010. Extreme deepening of the Atlantic overturning circulation during deglaciation. Nature Geosci 3, 567–571. https://doi.org/10.1038/ngeo921

Barras, C., Fontanier, C., Jorissen, F., Hohenegger, J., 2010. A comparison of spatial and temporal variability of living benthic foraminiferal faunas at 550m depth in the Bay of Biscay. Micropaleontology 56, 275–295.

Bauch, H.A., Erlenkeuser, H., Spielhagen, R.F., Struck, U., Matthiessen, J., Thiede, J., Heinemeier, J., 2001. A multiproxy reconstruction of the evolution of deep and surface waters

in the subarctic Nordic seas over the last 30,000yr. Quaternary Science Reviews 20, 659–678. https://doi.org/10.1016/S0277-3791(00)00098-6

Bayon, G., Dennielou, B., Etoubleau, J., Ponzevera, E., Toucanne, S., Bermell, S., 2012. Intensifying Weathering and Land Use in Iron Age Central Africa. Science 335, 1219–1222. https://doi.org/10.1126/science.1215400

Bernhard, J.M., Alve, E., 1996. Survival, ATP pool, and ultrastructural characterization of benthic foraminifera from Drammensfjord (Norway): response to anoxia. Marine Micropaleontology 28, 5–17. https://doi.org/10.1016/0377-8398(95)00036-4

Blaser, P., Pöppelmeier, F., Schulz, H., Gutjahr, M., Frank, M., Lippold, J., Heinrich, H., Link, J.M., Hoffmann, J., Szidat, S., Frank, N., 2019. The resilience and sensitivity of Northeast Atlantic deep water εNd to overprinting by detrital fluxes over the past 30,000 years. Geochimica et Cosmochimica Acta 245, 79–97. https://doi.org/10.1016/j.gca.2018.10.018

Boavida, J., Becheler, R., Choquet, M., Frank, N., Taviani, M., Bourillet, J.-F., Meistertzheim, A.-L., Grehan, A., Savini, A., Arnaud-Haond, S., 2019. Out of the Mediterranean? Post-glacial colonization pathways varied among cold-water coral species. Journal of Biogeography 46, 915–931. https://doi.org/10.1111/jbi.13570

Bock, M.J., Mayer, L.M., 2000. Mesodensity organo–clay associations in a near-shore sediment. Marine Geology 163, 65–75. https://doi.org/10.1016/S0025-3227(99)00105-X

Boers, N., Ghil, M., Rousseau, D. D., 2018. Ocean circulation, ice shelf, and sea ice interactions explain Dansgaard–Oeschger cycles. PNAS 115, E11005–E11014. https://doi.org/10.1073/pnas.1802573115

Bond, G., Heinrich, H., Broecker, W., Labeyrie, L., McManus, J., Andrews, J., Huon, S., Jantschik, R., Clasen, S., Simet, C., Tedesco, K., Klas, M., Bonani, G., Ivy, S., 1992. Evidence for massive discharges of icebergs into the North Atlantic ocean during the last glacial period. Nature 360, 245–249. https://doi.org/10.1038/360245a0

Borja, A., Amouroux, D., Anschutz, P., Gómez-Gesteira, M., Uyarra, M.C., Valdés, L., 2019. Chapter 5 - The Bay of Biscay, in: Sheppard, C. (Ed.), World Seas: An Environmental Evaluation (Second Edition). Academic Press, pp. 113–152. https://doi.org/10.1016/B978-0-12-805068-2.00006-1

Boswell, S.M., Toucanne, S., Pitel-Roudaut, M., Creyts, T.T., Eynaud, F., Bayon, G., 2019. Enhanced surface melting of the Fennoscandian Ice Sheet during periods of North Atlantic cooling. Geology 47, 664–668. https://doi.org/10.1130/G46370.1

Bourillet, J. F., Migeon, S., Damy, G., 2001. Le carottage à bord du N/O Le Suroît – Mission ESSCAR-7. IFREMER R.INT.DRO/GM/2001-10, 42

Bourillet, J.-F., Zaragosi, S., Mulder, T., 2006. The French Atlantic margin and deep-sea submarine systems. Geo-Mar Lett 26, 311–315. https://doi.org/10.1007/s00367-006-0042-2

Bouvier, A., Vervoort, J.D., Patchett, P.J., 2008. The Lu–Hf and Sm–Nd isotopic composition of CHUR: Constraints from unequilibrated chondrites and implications for the bulk composition of terrestrial planets. Earth and Planetary Science Letters 273, 48–57. https://doi.org/10.1016/j.epsl.2008.06.010

Brady, E.C., Otto-Bliesner, B.L., 2011. The role of meltwater-induced subsurface ocean warming in regulating the Atlantic meridional overturning in glacial climate simulations. Clim Dyn 37, 1517–1532. https://doi.org/10.1007/s00382-010-0925-9

Brendryen, J., Haflidason, H., Yokoyama, Y., Haaga, K. A., & Hannisdal, B., 2020. Eurasian Ice Sheet collapse was a major source of Meltwater Pulse 1A 14,600 years ago. Nature Geoscience, 13(5), 363-368.

Broecker, W.S., 1991. The Great Ocean Conveyor. Oceanography 4, 79–89.

Broecker, W.S., Denton, G.H., 1990. The role of ocean-atmosphere reorganizations in glacial cycles. Quaternary Science Reviews 9, 305–341. https://doi.org/10.1016/0277-3791(90)90026-7

Buzas, M.A., 1990. Another look at confidence limits for species proportions. Journal of Paleontology 64, 842–843. https://doi.org/10.1017/S002233600001903X

Cacho, I., Grimalt, J. O., Pelejero, C., Canals, M., Sierro, F. J., Flores, J. A., & Shackleton, N. 1999. Dansgaard-Oeschger and Heinrich event imprints in Alboran Sea paleotemperatures. Paleoceanography, 14(6), 698-705.

Caralp, M., Lamy, A., Pujos, M., 1970. Contribution a la Connaissance de la Distribution bathymetrique des Foraminiferes dans le Golfe de Gascogne. Revista Española de Micropaleontologia 2, 55–84.

Chapman, M.R., Shackleton, N.J., 1998. Millennial-scale fluctuations in North Atlantic heat flux during the last 150,000 years. Earth and Planetary Science Letters 159, 57–70. https://doi.org/10.1016/S0012-821X(98)00068-5

Clark, P. U., Shakun, J. D., Baker, P. A., Bartlein, P. J., Brewer, S., Brook, E., ... & Williams, J. W., 2012. Global climate evolution during the last deglaciation. Proceedings of the National Academy of Sciences, 109(19), E1134-E1142.

Colin, C., Tisnérat-Laborde, N., Mienis, F., Collart, T., Pons-Branchu, E., Dubois-Dauphin, Q., Frank, N., Dapoigny, A., Ayache, M., Swingedouw, D., Dutay, J.-C., Eynaud, F., Debret, M., Blamart, D., Douville, E., 2019. Millennial-scale variations of the Holocene North Atlantic mid-depth gyre inferred from radiocarbon and neodymium isotopes in cold water corals. Quat. Sci. Rev. 211, 93–106. https://doi.org/10.1016/j.quascirev.2019.03.011

Copard, K., Colin, C., Frank, N., Jeandel, C., Montero Serrano, J.-C., Reverdin, G., Ferron, B., 2011. Nd isotopic composition of water masses and dilution of the Mediterranean outflow along the southwest European margin. Geochemistry, Geophysics, Geosystems 12. https://doi.org/10.1029/2011GC003529

Dansgaard, W., Johnsen, S.J., Clausen, H.B., Dahl-Jensen, D., Gundestrup, N.S., Hammer, C.U., Hvidberg, C.S., Steffensen, J.P., Sveinbjörnsdottir, A.E., Jouzel, J., Bond, G., 1993. Evidence for general instability of past climate from a 250-kyr ice-core record. Nature 364, 218–220. https://doi.org/10.1038/364218a0

Denton, G., Anderson, R., Toggweiler, J.R., Edwards, R., Schaefer, J., Putnam, A., 2010. The Last Glacial Termination. Science (New York, N.Y.) 328, 1652–6. https://doi.org/10.1126/science.1184119

Denton, G.H., Toucanne, S., Putnam, A.E., Barrell, D.J.A., Russell, J.L., 2022. Heinrich summers. Quaternary Science Reviews 295, 107750. https://doi.org/10.1016/j.quascirev.2022.107750

Depuydt, P., Mojtahid, M., Barras, C., Bouhdayad, F.Z., Toucanne, S., 2022. Intermediate ocean circulation and cryosphere dynamics in the northeast Atlantic during Heinrich Stadials: benthic foraminiferal assemblage response. Journal of Quaternary Science 37, 1207–1221. https://doi.org/10.1002/jqs.3444

Depuydt, P., Barras, C., Toucanne, S., Fossile, E., Mojtahid, M., 2023. Implication of size fraction on benthic foraminiferal-based paleo-reconstructions: a case study from the Bay of Biscay (NE Atlantic). Marine Micropaleontology

Dickson, R.R., Brown, J., 1994. The production of North Atlantic Deep Water: Sources, rates, and pathways. Journal of Geophysical Research: Oceans 99, 12319–12341. https://doi.org/10.1029/94JC00530

Duchemin, G., Jorissen, F.J., Le Loc'h, F., Andrieux-Loyer, F., Hily, C., Thouzeau, G., 2008. Seasonal variability of living benthic foraminifera from the outer continental shelf of the Bay of Biscay. Journal of Sea Research 59, 297–319. https://doi.org/10.1016/j.seares.2008.03.006

Duplessy, J.C., 1981. CEPAG cruise,Le Suroît R/V. https://doi.org/10.17600/81005011

Duros, P., Fontanier, C., de Stigter, H.C., Cesbron, F., Metzger, E., Jorissen, F.J., 2012. Live and dead benthic foraminiferal faunas from Whittard Canyon (NE Atlantic): Focus on taphonomic processes and paleo-environmental applications. Marine Micropaleontology 94–95, 25–44. https://doi.org/10.1016/j.marmicro.2012.05.004

Duros, P., Fontanier, C., Metzger, E., Pusceddu, A., Cesbron, F., de Stigter, H.C., Bianchelli, S., Danovaro, R., Jorissen, F.J., 2011. Live (stained) benthic foraminifera in the Whittard Canyon, Celtic margin (NE Atlantic). Deep Sea Research Part I: Oceanographic Research Papers 58, 128–146. https://doi.org/10.1016/j.dsr.2010.11.008

Ehlers, J., Gibbard, P.L., Hughes, P.D., 2011. Quaternary Glaciations - Extent and Chronology, Volume 15 - 1st Edition. Elsevier.

Fatela, F., Taborda, R., 2002. Confidence limits of species proportions in microfossil assemblages. Marine Micropaleontology 45, 169–174. https://doi.org/10.1016/S0377-8398(02)00021-X

Ferrer, L., Caballero, A., 2011. Eddies in the Bay of Biscay: A numerical approximation. Journal of Marine Systems 87, 133–144. https://doi.org/10.1016/j.jmarsys.2011.03.008

Fontanier, C., Jorissen, F., Anschutz, P., Chaillou, G., 2006. Seasonal variability of benthic foraminiferal faunas at 1000 m depth in the Bay of Biscay. Journal of Foraminiferal Research 36, 61–76. https://doi.org/10.2113/36.1.61

Fontanier, C., Jorissen, F.J., Chaillou, G., David, C., Anschutz, P., Lafon, V., 2003. Seasonal and interannual variability of benthic foraminiferal faunas at 550m depth in the Bay of Biscay.

Deep Sea Research Part I: Oceanographic Research Papers 50, 457–494. https://doi.org/10.1016/S0967-0637(02)00167-X

Fontanier, C., Jorissen, F.J., Licari, L., Alexandre, A., Anschutz, P., Carbonel, P., 2002. Live benthic foraminiferal faunas from the Bay of Biscay: faunal density, composition, and microhabitats. Deep Sea Research Part I: Oceanographic Research Papers 49, 751–785. https://doi.org/10.1016/S0967-0637(01)00078-4

Frigola, J., Moreno, A., Cacho, I., Canals, M., Sierro, F.J., Flores, J.A., Grimalt, J.O., 2008. Evidence of abrupt changes in Western Mediterranean Deep Water circulation during the last 50kyr: A high-resolution marine record from the Balearic Sea. Quaternary International, The Last 15ka of Environmental Change in Mediterranean Regions - Interpreting Different Archives 181, 88–104. https://doi.org/10.1016/j.quaint.2007.06.016

Frigola, J., Moreno, A., Cacho, I., Canals, M., Sierro, F.J., Flores, J.A., Grimalt, J.O., Hodell, D.A., Curtis, J.H., 2007. Holocene climate variability in the western Mediterranean region from a deepwater sediment record. Paleoceanography 22. https://doi.org/10.1029/2006PA001307

Friocourt, Y., Levier, B., Speich, S., Blanke, B., Drijfhout, S.S., 2007. A regional numerical ocean model of the circulation in the Bay of Biscay. Journal of Geophysical Research: Oceans 112. https://doi.org/10.1029/2006JC003835

Gooday, A.J., Hughes, J.A., 2002. Foraminifera associated with phytodetritus deposits at a bathyal site in the northern Rockall Trough (NE Atlantic): seasonal contrasts and a comparison of stained and dead assemblages. Marine Micropaleontology 46, 83–110. https://doi.org/10.1016/S0377-8398(02)00050-6

Grimm, E.C., Jacobson, G.L., Watts, W.A., Hansen, B.C.S., Maasch, K.A., 1993. A 50,000-Year Record of Climate Oscillations from Florida and Its Temporal Correlation with the Heinrich Events. Science 261, 198–200. https://doi.org/10.1126/science.261.5118.198

Grousset, F.E., Pujol, C., Labeyrie, L., Auffret, G., Boelaert, A., 2000. Were the North Atlantic Heinrich events triggered by the behavior of the European ice sheets? Geology 28, 123–126. https://doi.org/10.1130/0091-7613(2000)28<123:WTNAHE>2.0.CO;2

Hall, I.R., McCave, I.N., 2000. Palaeocurrent reconstruction, sediment and thorium focussing on the Iberian margin over the last 140 ka. Earth and Planetary Science Letters 178, 151–164. https://doi.org/10.1016/S0012-821X(00)00068-6

Hammer, O., Harper, D.A.T., Ryan, P.D., 2001. PAST: Paleontological Statistics Software Package for Education and Data Analysis 9.

Hayek, L.-A., Buzas, M., 1997. Surveying Natural Populations: Quantitative Tools for Assessing Biodiversity, Surveying Natural Populations. Columbia University Press. https://doi.org/10.7312/haye14620

Heinrich, H., 1988. Origin and consequences of cyclic ice rafting in the northeast Atlantic Ocean during the past 130,000 years. Quaternary research, 29(2), 142-152.

Hemming, S.R., 2004. Heinrich events: Massive late Pleistocene detritus layers of the North Atlantic and their global climate imprint. Reviews of Geophysics 42. https://doi.org/10.1029/2003RG000128

Herguera, J.C., Berger, W.H., 1991. Paleoproductivity from benthic foraminifera abundance: Glacial to postglacial change in the west-equatorial Pacific. Geology 19, 1173–1176. https://doi.org/10.1130/0091-7613(1991)019<1173:PFBFAG>2.3.CO;2

Hermelin, J.O.R., Shimmield, G.B., 1990. The importance of the oxygen minimum zone and sediment geochemistry in the distribution of Recent benthic foraminifera in the northwest Indian Ocean. Marine Geology 91, 1–29. https://doi.org/10.1016/0025-3227(90)90130-C

Hillaire-Marcel, C., de Vernal, A., Bilodeau, G., Weaver, A.J., 2001. Absence of deep-water formation in the Labrador Sea during the last interglacial period. Nature 410, 1073–1077. https://doi.org/10.1038/35074052

Hoogakker, B.A.A., Chapman, M.R., McCave, I.N., Hillaire-Marcel, C., Ellison, C.R.W., Hall, I.R., Telford, R.J., 2011. Dynamics of North Atlantic Deep Water masses during the Holocene. Paleoceanography 26. https://doi.org/10.1029/2011PA002155

Huthnance, J.M., 1986. The Rockall slope current and shelf-edge processes. Proceedings of the Royal Society of Edinburgh, Section B: Biological Sciences 88, 83–101. https://doi.org/10.1017/S0269727000004486

Huthnance, J.M., 1984. Slope Currents and "JEBAR." Journal of Physical Oceanography 14, 795–810. https://doi.org/10.1175/1520-0485(1984)014<0795:SCA>2.0.CO;2

Huthnance, J.M., Inall, M.E., Fraser, N.J., 2020. Oceanic Density/Pressure Gradients and Slope Currents. Journal of Physical Oceanography 50, 1643–1654. https://doi.org/10.1175/JPO-D-19-0134.1

Ivanovic, R.F., Gregoire, L.J., Burke, A., Wickert, A.D., Valdes, P.J., Ng, H.C., Robinson, L.F., McManus, J.F., Mitrovica, J.X., Lee, L., Dentith, J.E., 2018. Acceleration of Northern Ice Sheet Melt Induces AMOC Slowdown and Northern Cooling in Simulations of the Early Last Deglaciation. Paleoceanography and Paleoclimatology 33, 807–824. https://doi.org/10.1029/2017PA003308

Jeandel, C., Oelkers, E.H., 2015. The influence of terrigenous particulate material dissolution on ocean chemistry and global element cycles. Chemical Geology 395, 50–66. https://doi.org/10.1016/j.chemgeo.2014.12.001

Jiménez-Espejo, F. J., Pardos-Gené, M., Martínez-Ruiz, F., García-Alix, A., Van de Flierdt, T., Toyofuku, T., ... & Kreissig, K., 2015. Geochemical evidence for intermediate water circulation in the westernmost Mediterranean over the last 20 kyr BP and its impact on the Mediterranean Outflow. Global and Planetary Change, 135, 38-46.

Jorissen, F.J., 1987. The distribution of benthic foraminifera in the Adriatic Sea. Marine Micropaleontology 12, 21–48. https://doi.org/10.1016/0377-8398(87)90012-0

Jouanneau, J.M., Weber, O., Cremer, M., Castaing, P., 1999. Fine-grained sediment budget on the continental margin of the Bay of Biscay. Deep Sea Research Part II: Topical Studies in Oceanography 46, 2205–2220. https://doi.org/10.1016/S0967-0645(99)00060-0

Keffer, T., Martinson, D.G., Corliss, B.H., 1988. The Position of the Gulf Stream During Quaternary Glaciations. Science 241, 440–442. https://doi.org/10.1126/science.241.4864.440

Keil, R.G., Tsamakis, E., Fuh, C.B., Giddings, J.C., Hedges, J.I., 1994. Mineralogical and textural controls on the organic composition of coastal marine sediments: Hydrodynamic separation using SPLITT-fractionation. Geochimica et Cosmochimica Acta 58, 879–893. https://doi.org/10.1016/0016-7037(94)90512-6

Koho, K.A., Piña-Ochoa, E., Geslin, E., Risgaard-Petersen, N., 2011. Vertical migration, nitrate uptake and denitrification: survival mechanisms of foraminifers (Globobulimina turgida) under low oxygen conditions. FEMS Microbiology Ecology 75, 273–283. https://doi.org/10.1111/j.1574-6941.2010.01010.x

Lacan, F., Jeandel, C., 2004. Neodymium isotopic composition and rare earth element concentrations in the deep and intermediate Nordic Seas: Constraints on the Iceland Scotland Overflow Water signature. Geochemistry, Geophysics, Geosystems 5. https://doi.org/10.1029/2004GC000742

Le Groupe Tourbillon, 1983. The Tourbillon experiment: a study of a mesoscale eddy in the eastern North Atlantic. Deep Sea Research Part A. Oceanographic Research Papers 30, 475–511. https://doi.org/10.1016/0198-0149(83)90086-9

Leduc, G., Vidal, L., Tachikawa, K., Rostek, F., Sonzogni, C., Beaufort, L., Bard, E., 2007. Moisture transport across Central America as a positive feedback on abrupt climatic changes. Nature 445, 908–911. https://doi.org/10.1038/nature05578

Lehman, S.J., Keigwin, L.D., 1992. Sudden changes in North Atlantic circulation during the last deglaciation. Nature 356, 757–762. https://doi.org/10.1038/356757a0

Liu, Z., Otto-Bliesner, B.L., He, F., Brady, E.C., Thomas, R., Clark, P.U., Carlson, A.E., Lynch-Stieglitz, J., Curry, W., Brook, E., Erickson, D., Jacob, R., Kutzbach, J., Cheng, J., 2009. Transient simulation of last deglaciation with a new mechanism for Bolling-Allerod warming. Science (New York, N.Y.) 325. https://doi.org/10.1126/science.1171041

Lozier, M.S., Li, F., Bacon, S., Bahr, F., Bower, A.S., Cunningham, S.A., Jong, M.F. de, Steur, L. de, deYoung, B., Fischer, J., Gary, S.F., Greenan, B.J.W., Holliday, N.P., Houk, A., Houpert, L., Inall, M.E., Johns, W.E., Johnson, H.L., Johnson, C., Karstensen, J., Koman, G., Bras, I.A.L., Lin, X., Mackay, N., Marshall, D.P., Mercier, H., Oltmanns, M., Pickart, R.S., Ramsey, A.L., Rayner, D., Straneo, F., Thierry, V., Torres, D.J., Williams, R.G., Wilson, C., Yang, J., Yashayaev, I., Zhao, J., 2019. A sea change in our view of overturning in the subpolar North Atlantic. Science 363, 516–521. https://doi.org/10.1126/science.aau6592

Lynch-Stieglitz, J., 2017. The Atlantic Meridional Overturning Circulation and Abrupt Climate Change. Annu. Rev. Mar. Sci. 9, 83–104. https://doi.org/10.1146/annurev-marine-010816-060415

Mackensen, A., Sejrup, H.P., Jansen, E., 1985. The distribution of living benthic foraminifera on the continental slope and rise off southwest Norway. Marine Micropaleontology 9, 275–306. https://doi.org/10.1016/0377-8398(85)90001-5

Marsh, R., Haigh, I.D., Cunningham, S.A., Inall, M.E., Porter, M., Moat, B.I., 2017. Large-scale forcing of the European Slope Current and associated inflows to the North Sea. Ocean Sci. 13. https://doi.org/10.5194/os-13-315-2017

Martínez-García, B., Pascual, A., Rodríguez-Lázaro, J., Bodego, A., 2013. Recent benthic foraminifers of the Basque continental shelf (Bay of Biscay, northern Spain): Oceanographic

implications. Continental Shelf Research 66, 105–122. https://doi.org/10.1016/j.csr.2013.07.006

Martinez-Lamas, R., Toucanne, S., Debret, M., Riboulot, V., Deloffre, J., Boissier, A., Cheron, S., Pitel, M., Bayon, G., Giosan, L., Soulet, G., 2020. Linking Danube River activity to Alpine Ice-Sheet fluctuations during the last glacial (ca. 33–17 ka BP): Insights into the continental signature of Heinrich Stadials. Quaternary Science Reviews 229, 106136. https://doi.org/10.1016/j.quascirev.2019.106136

McCave, I.N., Andrews, J.T., 2019. Distinguishing current effects in sediments delivered to the ocean by ice. II. Glacial to Holocene changes in high latitude North Atlantic upper ocean flows. Quaternary Science Reviews 223, 105902. https://doi.org/10.1016/j.quascirev.2019.105902

McCave, I.N., Manighetti, B., Robinson, S.G., 1995. Sortable silt and fine sediment size/composition slicing: Parameters for palaeocurrent speed and palaeoceanography. Paleoceanography 10, 593–610. https://doi.org/10.1029/94PA03039

McManus, J.F., Francois, R., Gherardi, J.-M., Keigwin, L.D., Brown-Leger, S., 2004. Collapse and rapid resumption of Atlantic meridional circulation linked to deglacial climate changes. Nature 428, 834–837. https://doi.org/10.1038/nature02494

Moffa-Sánchez, P., Moreno-Chamarro, E., Reynolds, D.J., Ortega, P., Cunningham, L., Swingedouw, D., Amrhein, D.E., Halfar, J., Jonkers, L., Jungclaus, J.H., Perner, K., Wanamaker, A., Yeager, S., 2019. Variability in the Northern North Atlantic and Arctic Oceans Across the Last Two Millennia: A Review. Paleoceanography and Paleoclimatology 34, 1399–1436. https://doi.org/10.1029/2018PA003508

Mojtahid, M., Griveaud, C., Fontanier, C., Anschutz, P., Jorissen, F.J., 2010. Live benthic foraminiferal faunas along a bathymetrical transect (140–4800m) in the Bay of Biscay (NE Atlantic). Revue de Micropaléontologie, Foraminiferal Geobiology 53, 139–162. https://doi.org/10.1016/j.revmic.2010.01.002

Mojtahid, M., Jorissen, F.J., Garcia, J., Schiebel, R., Michel, E., Eynaud, F., Gillet, H., Cremer, M., Diz Ferreiro, P., Siccha, M., Howa, H., 2013. High resolution Holocene record in the southeastern Bay of Biscay: Global versus regional climate signals. Palaeogeography, Palaeoclimatology, Palaeoecology 377, 28–44. https://doi.org/10.1016/j.palaeo.2013.03.004

Mojtahid, M., Toucanne, S., Fentimen, R., Barras, C., Le Houedec, S., Soulet, G., Bourillet, J.-F., Michel, E., 2017. Changes in northeast Atlantic hydrology during Termination 1: Insights

from Celtic margin's benthic foraminifera. Quaternary Science Reviews 175, 45–59. https://doi.org/10.1016/j.quascirev.2017.09.003

Moritz, M., Jochumsen, K., Kieke, D., Klein, B., Klein, H., Köllner, M., Rhein, M., 2021. Volume Transport Time Series and Variability of the North Atlantic Eastern Boundary Current at Goban Spur. Journal of Geophysical Research: Oceans 126, e2021JC017393. https://doi.org/10.1029/2021JC017393

Mulder, T., Zaragosi, S., Garlan, T., Mavel, J., Cremer, M., Sottolichio, A., Sénéchal, N., Schmidt, S., 2012. Present deep-submarine canyons activity in the Bay of Biscay (NE Atlantic). Marine Geology 295–298, 113–127. https://doi.org/10.1016/j.margeo.2011.12.005

Ng, H.C., Robinson, L.F., McManus, J.F., Mohamed, K.J., Jacobel, A.W., Ivanovic, R.F., Gregoire, L.J., Chen, T., 2018. Coherent deglacial changes in western Atlantic Ocean circulation. Nat Commun 9, 2947. https://doi.org/10.1038/s41467-018-05312-3

Orvik, K.A., Niiler, P., 2002. Major pathways of Atlantic water in the northern North Atlantic and Nordic Seas toward Arctic. Geophysical Research Letters 29, 2-1-2–4. https://doi.org/10.1029/2002GL015002

Otto-Bliesner, B.L., Brady, E.C., Clauzet, G., Tomas, R., Levis, S., Kothavala, Z., 2006. Last Glacial Maximum and Holocene Climate in CCSM3. Journal of Climate 19, 2526–2544. https://doi.org/10.1175/JCLI3748.1

Pascual, A., Rodríguez-Lázaro, J., Martínez-García, B., Varela, Z., 2020. Palaeoceanographic and palaeoclimatic changes during the last 37,000 years detected in the SE Bay of Biscay based on benthic foraminifera. Quaternary International, Quaternary Research in Spain: Environmental Changes and Human Footprint 566–567, 323–336. https://doi.org/10.1016/j.quaint.2020.03.043

Pascual, A., Rodriguez-Lazaro, J., Martín-Rubio, M., Jouanneau, J.-M., Weber, O., 2008. A survey of the benthic microfauna (foraminifera, Ostracoda) on the Basque shelf, southern Bay of Biscay. Journal of Marine Systems, Oceanography of the Bay of Biscay 72, 35–63. https://doi.org/10.1016/j.jmarsys.2007.05.015

Peck, V.L., Hall, I.R., Zahn, R., Elderfield, H., Grousset, F., Hemming, S.R., Scourse, J.D., 2006. High resolution evidence for linkages between NW European ice sheet instability and Atlantic Meridional Overturning Circulation. Earth and Planetary Science Letters 243, 476–488. https://doi.org/10.1016/j.epsl.2005.12.023

Peck, V.L., Hall, I.R., Zahn, R., Grousset, F., Hemming, S.R., Scourse, J.D., 2007. The relationship of Heinrich events and their European precursors over the past 60ka BP: a multi-proxy ice-rafted debris provenance study in the North East Atlantic. Quaternary Science Reviews 26, 862–875. https://doi.org/10.1016/j.quascirev.2006.12.002

Peltier, W.R., Vettoretti, G., 2014. Dansgaard-Oeschger oscillations predicted in a comprehensive model of glacial climate: A "kicked" salt oscillator in the Atlantic. Geophysical Research Letters 41, 7306–7313. https://doi.org/10.1002/2014GL061413

Piepgras, D. J., & Wasserburg, G. J. 1983. Influence of the Mediterranean outflow on the isotopic composition of neodymium in waters of the North Atlantic. Journal of Geophysical Research: Oceans, 88(C10), 5997-6006.

Piepgras, D.J., Wasserburg, G.J., 1987. Rare earth element transport in the western North Atlantic inferred from Nd isotopic observations. Geochimica et Cosmochimica Acta 51, 1257–1271. https://doi.org/10.1016/0016-7037(87)90217-1

Pina-Ochoa, E., Hogslund, S., Geslin, E., Cedhagen, T., Revsbech, N.P., Nielsen, L.P., Schweizer, M., Jorissen, F., Rysgaard, S., Risgaard-Petersen, N., 2010. Widespread occurrence of nitrate storage and denitrification among Foraminifera and Gromiida. Proceedings of the National Academy of Sciences 107, 1148–1153. https://doi.org/10.1073/pnas.0908440107

Pingree, R.D., Le Cann, B., 1992. Three anticyclonic slope water oceanic eDDIES (SWODDIES) in the Southern Bay of Biscay in 1990. Deep Sea Research Part A. Oceanographic Research Papers 39, 1147–1175. https://doi.org/10.1016/0198-0149(92)90062-X

Pingree, R.D., Le Cann, B., 1990. Structure, strength and seasonality of the slope currents in the Bay of Biscay region. Journal of the Marine Biological Association of the United Kingdom 70, 857–885. https://doi.org/10.1017/S0025315400059117

Pingree, R.D., Le Cann, B., 1989. Celtic and Armorican slope and shelf residual currents. Progress in Oceanography 23, 303–338. https://doi.org/10.1016/0079-6611(89)90003-7

Pollard, R. T., Griffttths, M. J., Cunningham, S. A., Read, J. F., Pérez, F. F., & Ríos, A. F., 1996. Vivaldi 1991-A study of the formation, circulation and ventilation of Eastern North Atlantic Central Water. Progress in Oceanography, 37(2), 167-192.

Pujos, 1972. Répartition des biocénoses de foraminifères benthiques sur le plateau continental du Golfe de Gascogne à l'ouest de l'embouchure de la Gironde. Revista Española de Micropaleontología 141–156.

Rahmstorf, S., 2002. Ocean circulation and climate during the past 120,000 years. Nature 419, 207–214. https://doi.org/10.1038/nature01090

Rasmussen, S.O., Andersen, K.K., Svensson, A.M., Steffensen, J.P., Vinther, B.M., Clausen, H.B., Siggaard-Andersen, M.-L., Johnsen, S.J., Larsen, L.B., Dahl-Jensen, D., Bigler, M., Röthlisberger, R., Fischer, H., Goto-Azuma, K., Hansson, M.E., Ruth, U., 2006. A new Greenland ice core chronology for the last glacial termination. Journal of Geophysical Research: Atmospheres 111. https://doi.org/10.1029/2005JD006079

Rasmussen, S.O., Bigler, M., Blockley, S.P., Blunier, T., Buchardt, S.L., Clausen, H.B., Cvijanovic, I., Dahl-Jensen, D., Johnsen, S.J., Fischer, H., Gkinis, V., Guillevic, M., Hoek, W.Z., Lowe, J.J., Pedro, J.B., Popp, T., Seierstad, I.K., Steffensen, J.P., Svensson, A.M., Vallelonga, P., Vinther, B.M., Walker, M.J.C., Wheatley, J.J., Winstrup, M., 2014. A stratigraphic framework for abrupt climatic changes during the Last Glacial period based on three synchronized Greenland ice-core records: refining and extending the INTIMATE event stratigraphy. Quaternary Science Reviews, Dating, Synthesis, and Interpretation of Palaeoclimatic Records and Model-data Integration: Advances of the INTIMATE project(INTegration of Ice-core, Marine and TErrestrial records, COST Action ES0907) 106, 14–28. https://doi.org/10.1016/j.quascirev.2014.09.007

Rasmussen, S.O., Seierstad, I.K., Andersen, K.K., Bigler, M., Dahl-Jensen, D., Johnsen, S.J., 2008. Synchronization of the NGRIP, GRIP, and GISP2 ice cores across MIS 2 and palaeoclimatic implications. Quaternary Science Reviews, INTegration of Ice-core, Marine and Terrestrial records (INTIMATE): Refining the record of the Last Glacial-Interglacial Transition 27, 18–28. https://doi.org/10.1016/j.quascirev.2007.01.016

Rasmussen, T.L., Thomsen, E., 2004. The role of the North Atlantic Drift in the millennial timescale glacial climate fluctuations. Palaeogeography, Palaeoclimatology, Palaeoecology 210, 101–116. https://doi.org/10.1016/j.palaeo.2004.04.005

Rhein, M., Kieke, D., Steinfeldt, R., 2015. Advection of North Atlantic Deep Water from the Labrador Sea to the southern hemisphere. Journal of Geophysical Research: Oceans 120, 2471–2487. https://doi.org/10.1002/2014JC010605

Risgaard-Petersen, N., Langezaal, A.M., Ingvardsen, S., Schmid, M.C., Jetten, M.S.M., Op den Camp, H.J.M., Derksen, J.W.M., Piña-Ochoa, E., Eriksson, S.P., Peter Nielsen, L., Peter Revsbech, N., Cedhagen, T., van der Zwaan, G.J., 2006. Evidence for complete denitrification in a benthic foraminifer. Nature 443, 93–96. https://doi.org/10.1038/nature05070

Rogerson, M., Rohling, E.J., Bigg, G.R., Ramirez, J., 2012. Paleoceanography of the Atlantic-Mediterranean exchange: Overview and first quantitative assessment of climatic forcing. Rev. Geophys. 50, RG2003. https://doi.org/10.1029/2011RG000376

Ruch, P., Mirmand, M., Jouanneau, J.-M., Latouche, C., 1993. Sediment budget and transfer of suspended sediment from the Gironde estuary to Cap Ferret Canyon. Marine Geology 111, 109–119. https://doi.org/10.1016/0025-3227(93)90191-W

Ruddiman, W.F., McIntyre, A., 1981. The North Atlantic Ocean during the last deglaciation. Palaeogeography, Palaeoclimatology, Palaeoecology 35, 145–214. https://doi.org/10.1016/0031-0182(81)90097-3

Rüggeberg, A., Dullo, C., Dorschel, B., Hebbeln, D., 2007. Environmental changes and growth history of a cold-water carbonate mound (Propeller Mound, Porcupine Seabight). Int J Earth Sci (Geol Rundsch) 96, 57–72. https://doi.org/10.1007/s00531-005-0504-1

Saha, R., 2015. Millennial-scale oscillations between sea ice and convective deep water formation. Paleoceanography 30, 1540–1555. https://doi.org/10.1002/2015PA002809

Sanchez Goñi, M.F., Cacho, I., Turon, J., Guiot, J., Sierro, F., Peypouquet, J., Grimalt, J., Shackleton, N., 2002. Synchroneity between marine and terrestrial responses to millennial scale climatic variability during the last glacial period in the Mediterranean region. Climate Dynamics 19, 95–105. https://doi.org/10.1007/s00382-001-0212-x

Schönfeld, J., 2006. Taxonomy and distribution of the Uvigerina peregrina plexus in the tropical to northeastern Atlantic. Journal of Foraminiferal Research 36, 355–367. https://doi.org/10.2113/gsjfr.36.4.355

Schönfeld, J., Altenbach, A.V., 2005. Late Glacial to Recent distribution pattern of deep-water Uvigerina species in the north-eastern Atlantic. Marine Micropaleontology 57, 1–24. https://doi.org/10.1016/j.marmicro.2005.05.004

Schönfeld, J., & Zahn, R. 2000. Late Glacial to Holocene history of the Mediterranean Outflow. Evidence from benthic foraminiferal assemblages and stable isotopes at the Portuguese margin. Palaeogeography, Palaeoclimatology, Palaeoecology, 159(1-2), 85-111.

Shaffer, G., Olsen, S.M., Bjerrum, C.J., 2004. Ocean subsurface warming as a mechanism for coupling Dansgaard-Oeschger climate cycles and ice-rafting events. Geophys. Res. Lett. 31, L24202. https://doi.org/10.1029/2004GL020968

Sicre, M.-A., Jalali, B., Eiríksson, J., Knudsen, K.-L., Klein, V., Pellichero, V., 2021. Trends and centennial-scale variability of surface water temperatures in the North Atlantic during the Holocene. Quaternary Science Reviews 265, 107033. https://doi.org/10.1016/j.quascirev.2021.107033

Sierro, F. J., D. A. Hodell, N. Andersen, L. A. Azibeiro, F. J. Jimenez-Espejo, A. Bahr, J. A. Flores, B. Ausin, M. Rogerson, and R. Lozano-Luz,2020. Mediterranean Overflow Over the Last 250 kyr: freshwater forcing from the tropics to the ice sheets, Paleoceanography and Paleoclimatology, 35(9), e2020PA003931

Singh, A.D., Rai, A.K., Tiwari, M., Naidu, P.D., Verma, K., Chaturvedi, M., Niyogi, A., Pandey, D., 2015. Fluctuations of Mediterranean Outflow Water circulation in the Gulf of Cadiz during MIS 5 to 7: Evidence from benthic foraminiferal assemblage and stable isotope records. Global and Planetary Change 133, 125–140. https://doi.org/10.1016/j.gloplacha.2015.08.005

Stanford, J.D., Rohling, E.J., Bacon, S., Roberts, A.P., Grousset, F.E., Bolshaw, M., 2011. A new concept for the paleoceanographic evolution of Heinrich event 1 in the North Atlantic. Quaternary Science Reviews 30, 1047–1066. https://doi.org/10.1016/j.quascirev.2011.02.003

Stumpf, R., Frank, M., Schönfeld, J., & Haley, B. A., 2010. Late Quaternary variability of Mediterranean outflow water from radiogenic Nd and Pb isotopes. Quaternary Science Reviews, 29(19-20), 2462-2472.

Sun, Y., Knorr, G., Zhang, X., Tarasov, L., Barker, S., Werner, M., Lohmann, G., 2022. Ice sheet decline and rising atmospheric CO2 control AMOC sensitivity to deglacial meltwater discharge. Global and Planetary Change 210, 103755. https://doi.org/10.1016/j.gloplacha.2022.103755

Tachikawa, K., Piotrowski, A.M., Bayon, G., 2014. Neodymium associated with foraminiferal carbonate as a recorder of seawater isotopic signatures. Quaternary Science Reviews 88, 1–13. https://doi.org/10.1016/j.quascirev.2013.12.027

Tanaka, T., Togashi, S., Kamioka, H., Amakawa, H., Kagami, H., Hamamoto, T., Yuhara, M., Orihashi, Y., Yoneda, S., Shimizu, H., Kunimaru, T., Takahashi, K., Yanagi, T., Nakano, T., Fujimaki, H., Shinjo, R., Asahara, Y., Tanimizu, M., Dragusanu, C., 2000. JNdi-1: a neodymium isotopic reference in consistency with LaJolla neodymium. Chemical Geology 168, 279–281. https://doi.org/10.1016/S0009-2541(00)00198-4

Tenzer, R., Gladkikh, V., 2014. Assessment of Density Variations of Marine Sediments with Ocean and Sediment Depths. The Scientific World Journal 2014, e823296. https://doi.org/10.1155/2014/823296

Thornalley, D.J.R., Barker, S., Becker, J., Hall, I.R., Knorr, G., 2013. Abrupt changes in deep Atlantic circulation during the transition to full glacial conditions. Paleoceanography 28, 253–262. https://doi.org/10.1002/palo.20025

Thornalley, D.J.R., Elderfield, H., McCave, I.N., 2009. Holocene oscillations in temperature and salinity of the surface subpolar North Atlantic. Nature 457, 711–714. https://doi.org/10.1038/nature07717

Toucanne, S., Soulet, G., Freslon, N., Jacinto, R.S., Dennielou, B., Zaragosi, S., Eynaud, F., Bourillet, J.-F., Bayon, G., 2015. Millennial-scale fluctuations of the European Ice Sheet at the end of the last glacial, and their potential impact on global climate. Quaternary Science Reviews 123, 113–133.

Toucanne, S., Soulet, G., Oliveiros, N.V., Boswell, S.M., Dennielou, B., Waelbroeck, C., Bayon, G., Mojtahid, M., Bosq, M., Sabine, M., Zaragosi, S., Bourillet, J.-F., Mercier, H., 2021. The North Atlantic Glacial Eastern Boundary Current as a Key Driver for Ice-Sheet—Amoc Interactions and Climate Instability. Paleoceanography and Paleoclimatology 36, e2020PA004068. https://doi.org/10.1029/2020PA004068

Toucanne, S., Zaragosi, S., Bourillet, J.-F., Marieu, V., Cremer, M., Kageyama, M., Van Vliet-Lanoë, B., Eynaud, F., Turon, J.-L., Gibbard, P.L., 2010. The first estimation of Fleuve Manche palaeoriver discharge during the last deglaciation: Evidence for Fennoscandian ice sheet meltwater flow in the English Channel ca 20–18ka ago. Earth and Planetary Science Letters 290, 459–473. https://doi.org/10.1016/j.epsl.2009.12.050

van Aken, 2000. The hydrography of the mid-latitude Northeast Atlantic Ocean: II: The intermediate water masses. Deep Sea Research Part I: Oceanographic Research Papers 47, 789–824. https://doi.org/10.1016/S0967-0637(99)00112-0

van de Flierdt, T., Griffiths, A.M., Lambelet, M., Little, S.H., Stichel, T., Wilson, D.J., 2016. Neodymium in the oceans: a global database, a regional comparison and implications for palaeoceanographic research. Philosophical Transactions of the Royal Society A: Mathematical, Physical and Engineering Sciences 374, 20150293. https://doi.org/10.1098/rsta.2015.0293

van Dijk, J. v., M. Ziegler, L. d. Nooijer, G. J. Reichart, C. Xuan, E. Ducassou, S. M. Bernasconi, and L. J. Lourens, 2018. A Saltier Glacial Mediterranean Outflow, Paleoceanography and Paleoclimatology, 33(2), 179-197

Vidal, L., Labeyrie, L., Cortijo, E., Arnold, M., Duplessy, J.C., Michel, E., Becqué, S., van Weering, T.C.E., 1997. Evidence for changes in the North Atlantic Deep Water linked to meltwater surges during the Heinrich events. Earth and Planetary Science Letters 146, 13–27. https://doi.org/10.1016/S0012-821X(96)00192-6

Voelker, A.H.L., Lebreiro, S.M., Schönfeld, J., Cacho, I., Erlenkeuser, H., Abrantes, F., 2006. Mediterranean outflow strengthening during northern hemisphere coolings: A salt source for the glacial Atlantic? Earth and Planetary Science Letters 245, 39-55

Webb, R.S., Rind, D.H., Lehman, S.J., Healy, R.J., Sigman, D., 1997. Influence of ocean heat transport on the climate of the Last Glacial Maximum. Nature 385, 695–699. https://doi.org/10.1038/385695a0

Weltje, G.J., Tjallingii, R., 2008. Calibration of XRF core scanners for quantitative geochemical logging of sediment cores: Theory and application. Earth and Planetary Science Letters 274, 423–438. https://doi.org/10.1016/j.epsl.2008.07.054

Zahn, R., Schönfeld, J., Kudrass, H.-R., Park, M.-H., Erlenkeuser, H., Grootes, P., 1997. Thermohaline instability in the North Atlantic during meltwater events: Stable isotope and ice-rafted detritus records from Core SO75-26KL, Portuguese Margin. Paleoceanography 12, 696–710. https://doi.org/10.1029/97PA00581

Zaragosi, S., Bourillet, J.-F., Eynaud, F., Toucanne, S., Denhard, B., Van Toer, A., Lanfumey, V., 2006. The impact of the last European deglaciation on the deep-sea turbidite systems of the

Celtic-Armorican margin (Bay of Biscay). Geo-Mar Lett 26, 317–329. https://doi.org/10.1007/s00367-006-0048-9

Zaragosi, S., Eynaud, F., Pujol, C., Auffret, G.A., Turon, J.-L., Garlan, T., 2001. Initiation of the European deglaciation as recorded in the northwestern Bay of Biscay slope environments (Meriadzek Terrace and Trevelyan Escarpment): a multi-proxy approach. Earth and Planetary Science Letters 188, 493–507. https://doi.org/10.1016/S0012-821X(01)00332-6

Zhang, X., Knorr, G., Lohmann, G., Barker, S., 2017. Abrupt North Atlantic circulation changes in response to gradual CO 2 forcing in a glacial climate state. Nature Geosci 10, 518–523. https://doi.org/10.1038/ngeo2974

Zou, S., Lozier, M.S., 2016. Breaking the Linkage Between Labrador Sea Water Production and Its Advective Export to the Subtropical Gyre. Journal of Physical Oceanography 46, 2169–2182. https://doi.org/10.1175/JPO-D-15-0210.1

9. Figure captions

Figure 1. Location of the study area. a) Figures showing the modern configuration of the study area. On the upper left panel, a figure modified from Depuydt et al. (2022) showing a 3D representation (N–S, W–E and in water depth) of the modern oceanic circulation in the North Atlantic representing the main currents (acronyms written in black), water masses (acronyms written in colours) and the subpolar (in blue) and subtropical (in red) gyres in the North Atlantic. On the right panel, bathymetric maps of the Bay of Biscay showing the modern circulation conditions, physiography, and the location of our study core SU81-44 (purple star), together with nearby upper slope sediment cores: MD95-2002 (brown star; Ménot et al., 2006; Eynaud et al., 2012; Toucanne et al., 2015), MD99-2328 (blue star; Mojtahid et al., 2017), BOBGEO-CS05 (orange star; Toucanne et al., 2021; Depuydt et al., 2022); PP10-12 (black star; Pascual et al., 2020). b) Bathymetric map showing the glacial conditions of the Bay of Biscay and the location of sediment cores, similarly to (a).

Figure 2. Chronostratigraphy of core SU81-44. a) NGRIP $\delta^{18}O$ (GICCS05 chronology; Rasmussen et al., 2006, 2014). b) Chronostratigraphic framework of core SU81-44 based on the synchronization of XRF-Ca/Ti ratios with cores MD95-2002 and BOBGEO-CS05 (Zaragosi et al., 2006; Toucanne et al., 2021; Depuydt et al., 2022). c) Percentages of the polar

planktonic species *N. pachyderma* in core SU81-44 (this study), core MD95-2002 (Grousset et al., 2000) and core BOBGEO-CS05 (Depuydt et al., 2022). The dashed purple line indicates the semi-quantitative analysis showing the absence of polar planktonic taxa in the top ~20 cm of core SU81-44 (J. Duprat: unpublished data). d) X-Ray photograph (see Figure S2 for the whole core) showing the ice-rafted debris (IRD) which allowed us to identify the Heinrich event 1. Purple diamonds indicate ^{14}C ages in core SU81-44 (cf. Figure S1).

Figure 3. Benthic foraminiferal data from core SU81-44. a) Benthic foraminiferal accumulation rates (BFAR; ind.cm^{-3}.ka^{-1}) for the >150 µm. b) Shannon index (H'). c-j) Relative abundances (%) of the fifteen most representative benthic foraminiferal species (>10 %). Full lines and dashed lines represent respectively, the >150 µm and >63 µm fractions. Greenland Interstadials (GI); grey bands: Heinrich Events (HEs); blue bands: Heinrich Stadial (HSs); orange band: Bølling-Allerød (BA); Marine Isotope Stage (MIS). The vertical dashed grey line represents the limit between early HS1 (ca. 18–16.7 ka) and late HS1 (ca. 16.7–14.7 ka). To better highlight the variations of the different species groups, the scale of the ordinate axis is not constant. Purple diamonds indicate ^{14}C ages in core SU81-44 (cf. Figure S1)

Figure 4. Abiotic data from core SU81-44. a) NGRIP δ18O (GICCS05 chronology; (Rasmussen et al., 2006, 2014). b) the most representative grain size distribution of our core. c) Median grain-size record (red line), silt/clay ratio (blue line) and UP10 (green line) as proxies for the reconstruction of CBDC flow speed changes (Frigola et al., 2007). d) Neodymium isotopic composition from planktonic foraminifera in core SU81-44 (expressed in ε_{Nd}). e) and f) respectively, $\delta^{18}O$ and $\delta^{13}C$ of benthic foraminifera (‰). Greenland Interstadials (GI); grey bands: Heinrich Events (HEs); blue bands: Heinrich Stadial (HSs); orange band: Bølling-Allerød (BA); Marine Isotope Stage (MIS). The vertical dashed grey line represents the limit between early HS1 (ca. 18.2–16.7 cal ka BP) and late HS1 (ca. 16.7–14.7 cal ka BP). Purple diamonds indicate ^{14}C ages in core SU81-44 (cf. Figure S1)

Figure 5. Reconstructions of slope current changes on the French Atlantic margin during the last 36 ka. a) Near-bottom flow speed on the upper slope (~1000 m) reconstructed from dimensionless UP10 data of the composite record of the northern Bay of Biscay (orange line)

and the core SU81-44 (black line); and from relative abundance of *T. angulosa* (dashed black line) in this study. b) Water mass signature from ε_{Nd} composite record of the northern Bay of Biscay (orange dashed line) and from this study (black line). c) Detritic Neodymium isotopic composition (ε_{Nd}; blue line) in core MD95-2002 (Toucanne et al., 2015). d) and e) respectively, $\delta^{18}O$ and $\delta^{13}C$ of benthic foraminifera (‰) from the upper slope composite record of the northern Bay of Biscay (orange line) and from this study (black line). Greenland Interstadials (GI); grey bands: Heinrich Events (HEs); blue bands: Heinrich Stadial (HSs); orange band: Bølling-Allerød (BA); Marine Isotope Stage (MIS). The vertical dashed grey line represents the limit between early HS1 (*i.e.* 18.2–16.7 ka) and late HS1 (*i.e.* 16.7–14.7 ka). R4 event represents a Channel River meltwater discharge during 20.3 ± 0.3 to 18.7 ± 0.3 ka (Toucanne et al., 2015). Purple diamonds indicate ^{14}C ages in core SU81-44 (cf. Figure S1)

10. Supplementary information

Figure S1. Age model of core SU81-44 based on synchronization of XRF-Ca/Ti ratios (full purple line) with cores MD95-2002 and BOBGEO-CS05 (Zaragosi et al., 2006; Toucanne et al., 2021; Depuydt et al., 2022). Sediment accumulation rate (SAR; dashed purple line) in SU81-44. Corrected ^{14}C ages (purple square) were calibrated using the atmospheric calibration curve IntCal20 (Reimer et al., 2020)

Figure S2. X-Ray radiographs of core SU81-44. Green box represents the worked sections in this study. Red box (S3) represents the unused section since it shows signs of core piston (red arrow).

Figure S3. PCA analysis based on covariance between the percentages of major species (>10 %).

Figure S4. Relative abundances (%) of the most representative benthic foraminiferal species (>10 %) in core SU81-44 (black line) and nearby cores: MD99-2328 (brown line; Mojtahid et al., 2017) and BOBGEO-CS05 (orange line; Depuydt et al., 2022). Full lines and dashed lines represent respectively, the >150 µm and >63 µm fractions. Greenland Interstadials (GI); grey

bands: Heinrich Events (HEs); blue bands: Heinrich Stadial (HSs); orange band: Bølling-Allerød (BA); Marine Isotope Stage (MIS). The vertical dashed grey line represents the limit between early HS1 (ca. 18.2–16.7 cal ka BP) and late HS1 (ca. 16.7–14.7 cal ka BP). To better highlight the variations of the different species groups, the scale of the ordinate axis is not constant.

Figure S5. Relative abundances (%) of the most representative benthic foraminiferal species (>10 %) in core SU81-44 (dashed black line) and the nearby core PP10-12 (blue line; Pascual et al., 2020) in the >63 µm fraction. Greenland Interstadials (GI), grey bands: Heinrich Events (HEs); blue bands: Heinrich Stadial (HSs); orange band: Bølling-Allerød (BA); Marine Isotope Stage (MIS). The vertical dashed grey line represents the limit between early HS1 (*i.e.* 18.2–16.7 ka) and late HS1 (*i.e.* 16.7–14.7 ka cal BP). To better highlight the variations of the different species groups, the scale of the ordinate axis is not constant.

Figure S6. Focus on HS2 in core SU81-44. a) Relative abundances (%) of the planktonic species N. pachyderma s. in core SU81-44 (black line; this study), BOBGEO-CS05 (orange line; Depuydt et al., 2022) and MD95-2002 (blue line; (Grousset et al., 2000). b) ($\overline{SS}$) composite records from the northern Bay of Biscay (Toucanne et al., 2021) and UP10 data from this study as proxies for the reconstruction of GEBC flow speed changes (Frigola et al., 2008; Toucanne et al., 2021). c) Relative abundances of high-energy indicator species (% *C. lobatulus* + % *T. angulosa*) in core SU81-44 (dashed black line; this study) and in core BOBGEO-CS05 (orange line; Depuydt et al., 2022). Dashed vertical line: Heinrich Event 2 (HE2) sensu-stricto according to the regional Ca/Ti synchronization (see Table S2 in Toucanne et al., 2021); blue bands: the HS2a,b cold events (Bard et al., 2000); yellow band: the mid-HS2 reventilation event. To better highlight the variations of the different species groups, the scale of the ordinate axis is not constant.

Table S1. Main tie-points for SU81-44 based on their synchronization to the reference core MD95-2002 (see age scale in Toucanne et al., 2021) with the XRF log (Ca/Ti) ratio. HS (HS1 to 3) refers to Heinrich Stadials. HE refers to Heinrich Event sensu-stricto (*i.e.* discharge of

iceberg from the Laurentide Ice Sheet to the Northeast Atlantic); GI- (1 to 7) refers to Greenland Interstadials. LGM- (1 to 7) refers to the Last Glacial Maximum.

Table S2. ^{14}C dates of core SU81-44 and calendar age range following age model of core MD95-2002.

Table S3. Benthic foraminiferal raw data available on https://doi.org/10.17882/91758

Highlights

- We present a continuous record of the European Slope Current for the last 36 kyr
- The slope current intensity peaks during the Bølling-Allerød then gradually decreases throughout the Holocene
- Changes in the meridional density gradient likely explain slope current changes
- Reappearance of the Mediterranean water in the southern Bay of Biscay at ~16 ka

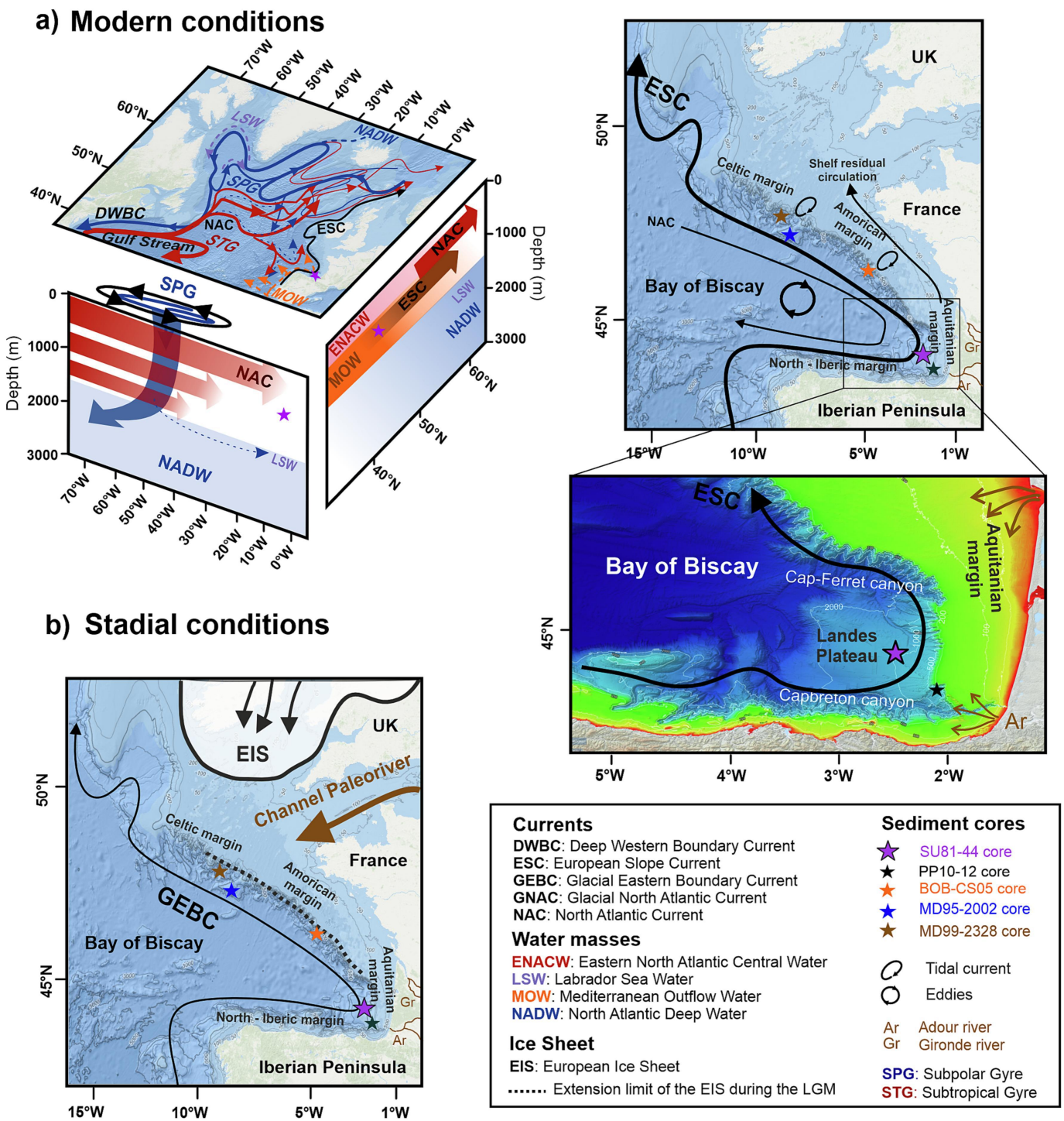
a) Modern conditions
LSW
NADW
SPG
DWBC
NAC
Gulf Stream
STG
ESC
MOW
ENACW
Depth (m)
b) Stadial conditions
EIS
UK
Channel Paleoriver
Celtic margin
France
Amorican margin
GEBC
Bay of Biscay
Aquitanian margin
North - Iberic margin
Iberian Peninsula
Shelf residual circulation
Cap-Ferret canyon
Landes Plateau
Capbreton canyon
Gr
Ar
Currents
DWBC: Deep Western Boundary Current
ESC: European Slope Current
GEBC: Glacial Eastern Boundary Current
GNAC: Glacial North Atlantic Current
NAC: North Atlantic Current
Water masses
ENACW: Eastern North Atlantic Central Water
LSW: Labrador Sea Water
MOW: Mediterranean Outflow Water
NADW: North Atlantic Deep Water
Ice Sheet
EIS: European Ice Sheet
Extension limit of the EIS during the LGM
Sediment cores
SU81-44 core
PP10-12 core
BOB-CS05 core
MD95-2002 core
MD99-2328 core
Tidal current
Eddies
Ar Adour river
Gr Gironde river
SPG: Subpolar Gyre
STG: Subtropical Gyre

Figure 1

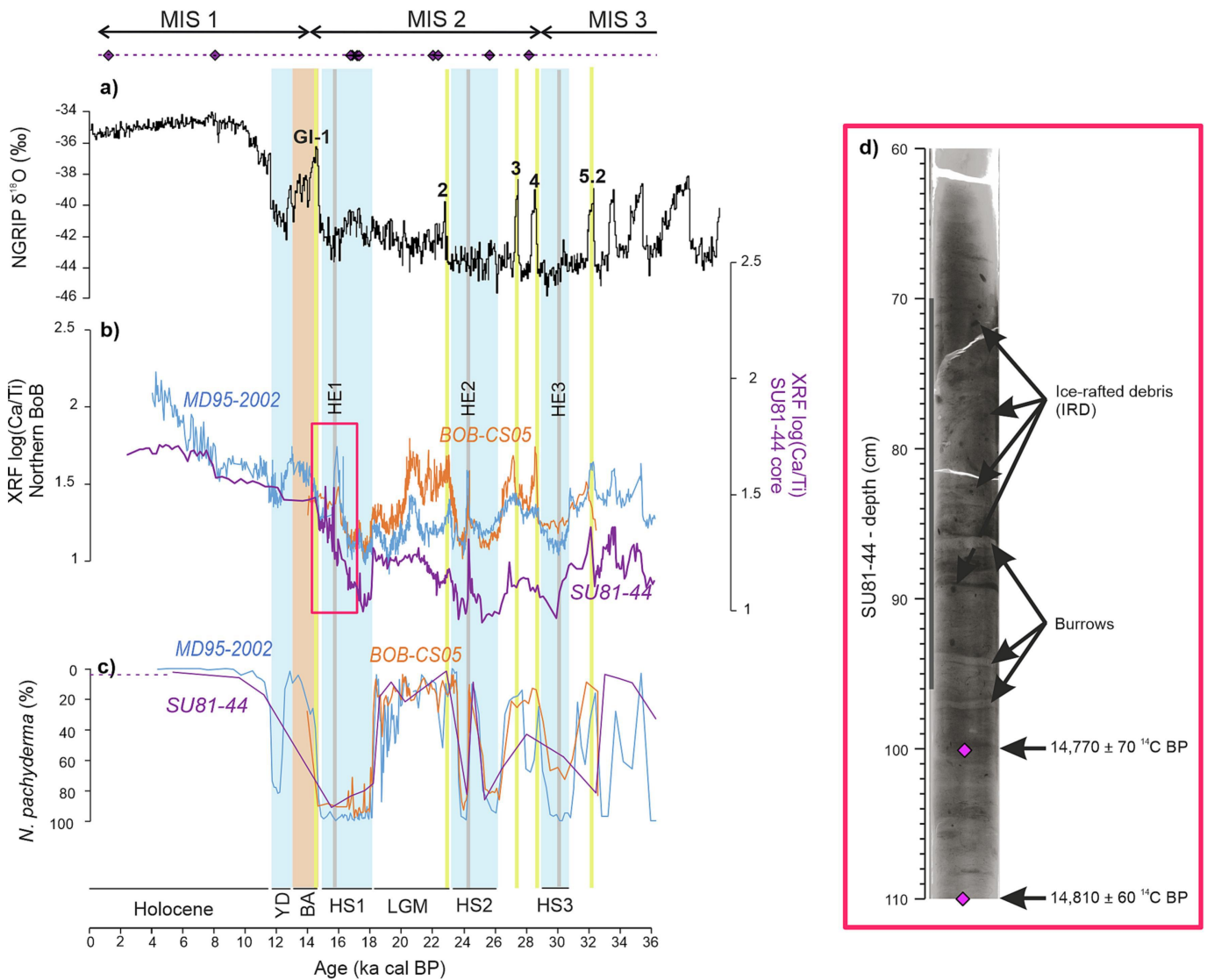
MIS 1
MIS 2
MIS 3
a)
NGRIP δ18O (‰)
-34
-36
-38
-40
-42
-44
-46
GI-1
2
3
4
5.2
b)
XRF log(Ca/Ti) Northern BoB
2.5
2
1.5
1
MD95-2002
BOB-CS05
SU81-44
HE1
HE2
HE3
XRF log(Ca/Ti) SU81-44 core
2.5
2
1.5
1
c)
N. pachyderma (%)
0
20
40
60
80
100
MD95-2002
BOB-CS05
SU81-44
Holocene
YD
BA
HS1
LGM
HS2
HS3
0 2 4 6 8 10 12 14 16 18 20 22 24 26 28 30 32 34 36
Age (ka cal BP)
d)
SU81-44 - depth (cm)
60
70
80
90
100
110
Ice-rafted debris (IRD)
Burrows
14,770 ± 70 14C BP
14,810 ± 60 14C BP

Figure 2

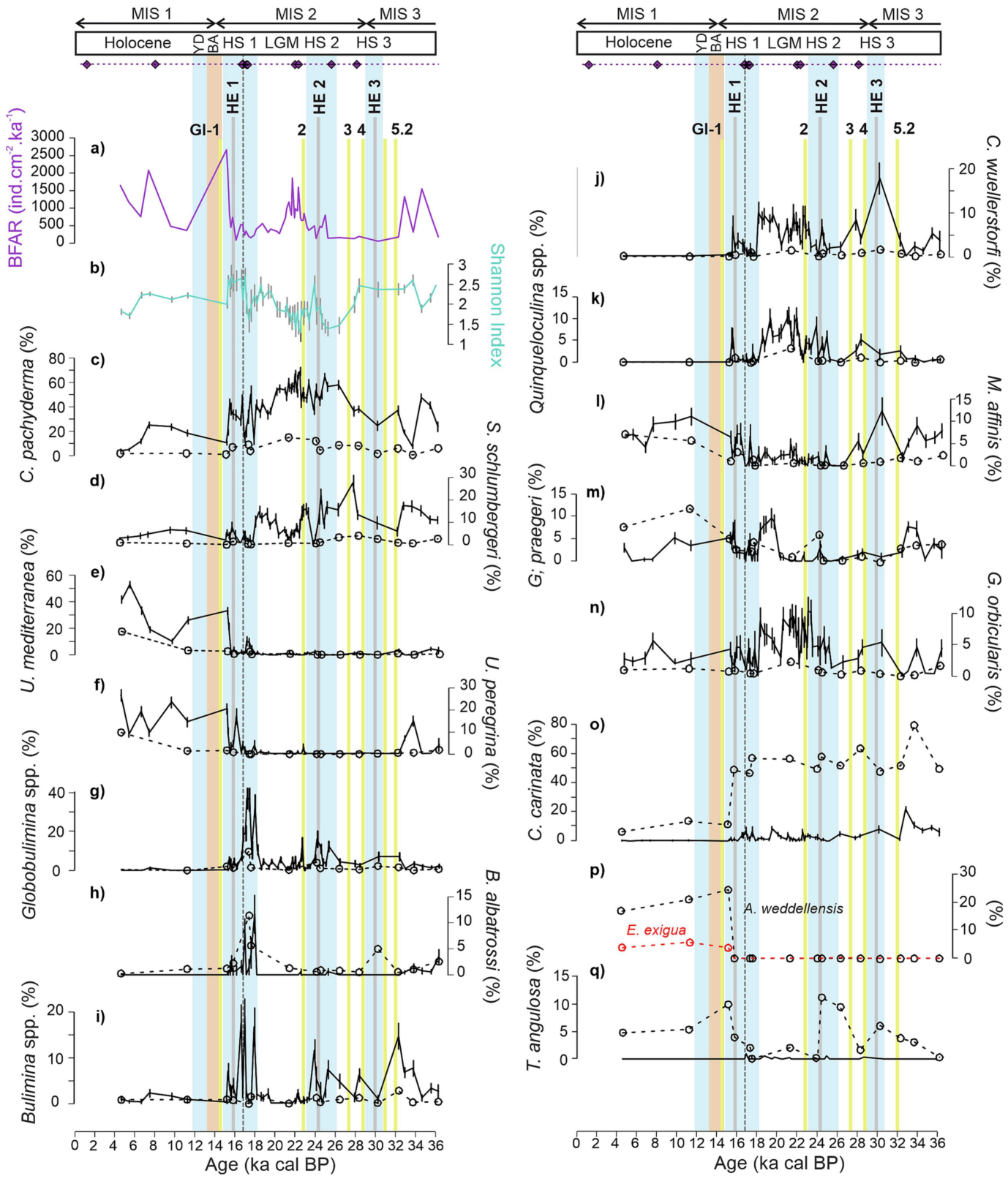
MIS 1
MIS 2
MIS 3
Holocene
YD
BA
HS 1
LGM
HS 2
HS 3
HE 1
HE 2
HE 3
GI-1
2
3
4
5.2
BFAR (ind.cm-2.ka-1)
Shannon Index
C. pachyderma (%)
S. schlumbergeri (%)
U. mediterranea (%)
U. peregrina (%)
Globobulimina spp. (%)
B. albatrossi (%)
Bulimina spp. (%)
Quinqueloculina spp. (%)
C. wuellerstorfi (%)
M. affinis (%)
G; praegeri (%)
G. orbicularis (%)
C. carinata (%)
A. weddellensis
E. exigua
T. angulosa (%)
Age (ka cal BP)

Figure 3

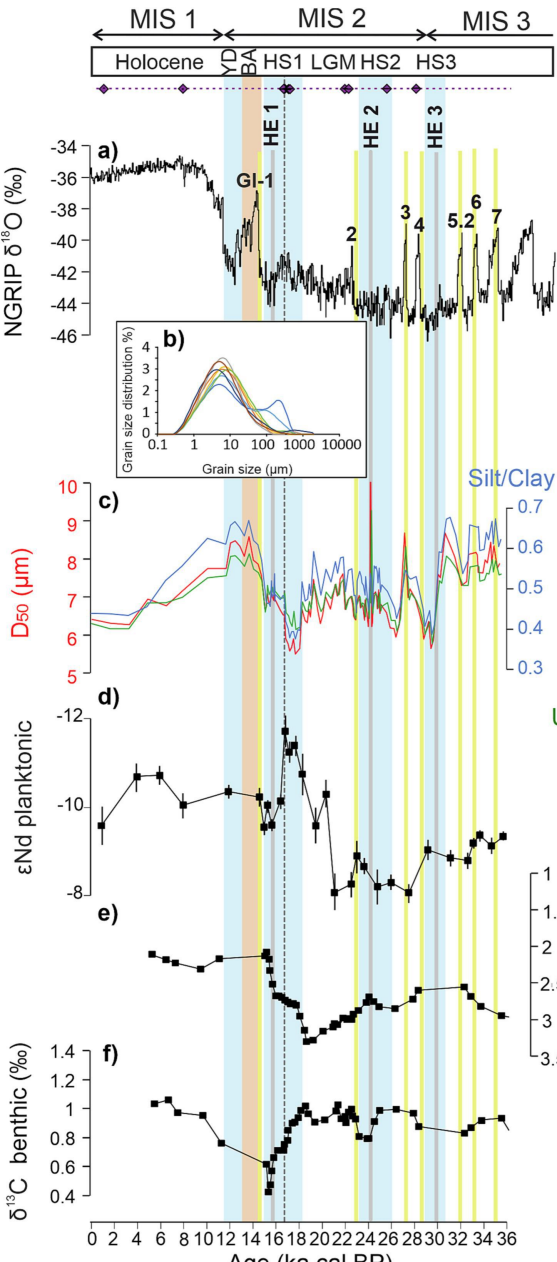
MIS 1
MIS 2
MIS 3
Holocene
YD
BA
HS1
LGM
HS2
HS3
HE 1
HE 2
HE 3
a)
NGRIP δ18O (‰)
-34
-36
-38
-40
-42
-44
-46
GI-1
2
3
4
5.2
6
7
b)
Grain size distribution (%)
Grain size (µm)
c)
D50 (µm)
Silt/Clay
d)
εNd planktonic
UP10 (%)
>10 µm
e)
δ18O benthic (‰)
f)
δ13C benthic (‰)
Age (ka cal BP)

Figure 4

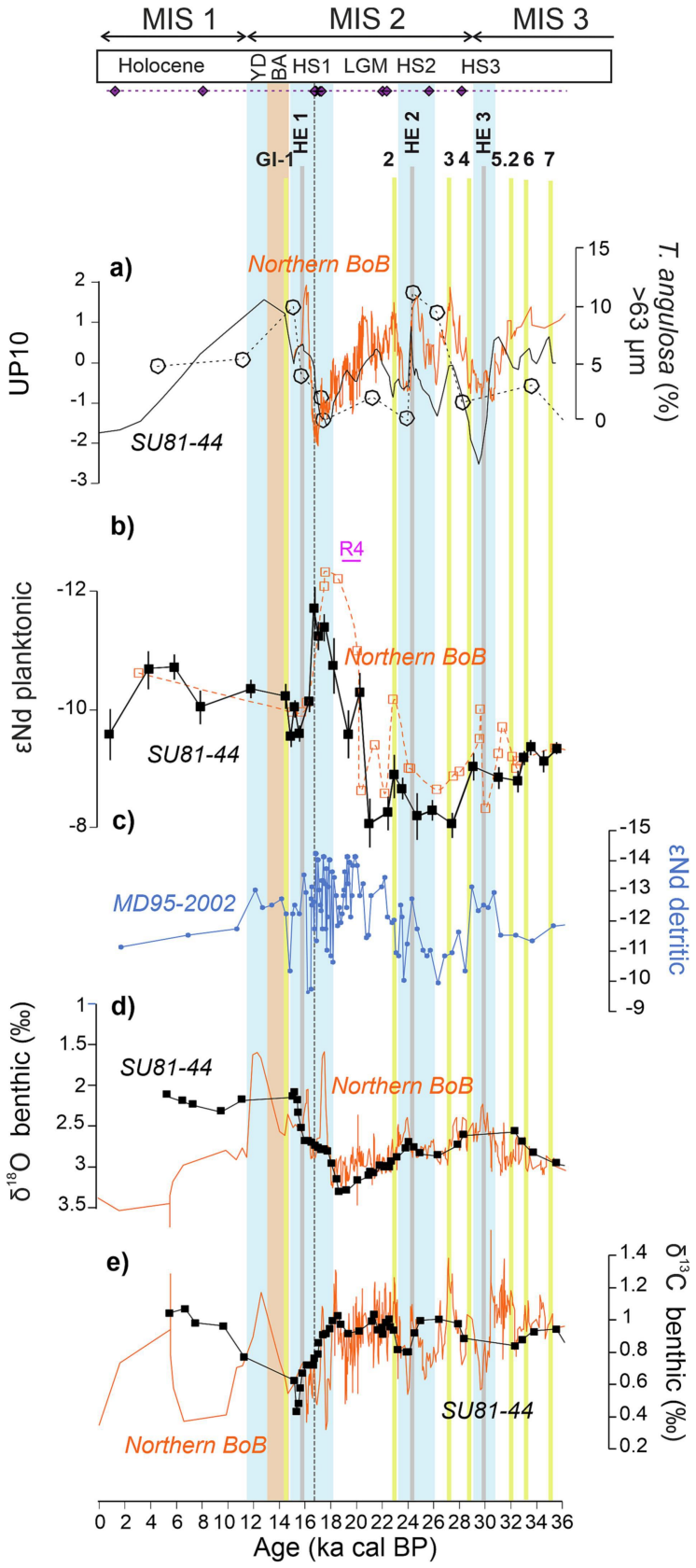
MIS 1
MIS 2
MIS 3
Holocene
YD
BA
HS1
LGM
HS2
HS3
GI-1
HE 1
2
HE 2
3 4
HE 3
5.2 6 7
a)
Northern BoB
SU81-44
UP10
T. angulosa (%) >63 µm
b)
R4
Northern BoB
SU81-44
εNd planktonic
c)
MD95-2002
εNd detritic
d)
SU81-44
Northern BoB
δ18O benthic (‰)
e)
SU81-44
Northern BoB
δ13C benthic (‰)
0 2 4 6 8 10 12 14 16 18 20 22 24 26 28 30 32 34 36
Age (ka cal BP)

Figure 5